

# The Dawn of the Red: Star formation histories of group galaxies over the past 5 billion years

Sean L. McGee<sup>1,2\*</sup>, Michael L. Balogh<sup>1</sup>, David J. Wilman<sup>3</sup>, Richard G. Bower<sup>2</sup>, John S. Mulchaey<sup>4</sup>, Laura C. Parker<sup>5</sup> and Augustus Oemler, Jr.<sup>4</sup>

<sup>1</sup>*Department of Physics and Astronomy, University of Waterloo, Waterloo, Ontario, N2L 3G1, Canada*

<sup>2</sup>*Department of Physics, University of Durham, Durham, UK, DH1 3LE*

<sup>3</sup>*Max-Planck-Institut für extraterrestrische Physik, Giessenbachstrasse 85748 Garching Germany*

<sup>4</sup>*Observatories of the Carnegie Institution, 813 Santa Barbara Street, Pasadena, California, USA*

<sup>5</sup>*Department of Physics and Astronomy, McMaster University, Hamilton, Ontario L8S 4M1, Canada*

8 November 2018

## ABSTRACT

We examine the star formation properties of group and field galaxies in two surveys, SDSS (at  $z \sim 0.08$ ) and GEEC (at  $z \sim 0.4$ ). Using UV imaging from the *GALEX* space telescope, along with optical and, for GEEC, near infrared photometry, we compare the observed spectral energy distributions to large suites of stellar population synthesis models. This allows us to accurately determine star formation rates and stellar masses. We find that star forming galaxies of all environments undergo a systematic lowering of their star formation rate between  $z=0.4$  and  $z=0.08$  regardless of mass. Nonetheless, the fraction of passive galaxies is higher in groups than the field at both redshifts. Moreover, the difference between the group and field grows with time and is mass-dependent, in the sense the the difference is larger at low masses. However, the star formation properties of star forming galaxies, as measured by their average specific star formation rates, are consistent within the errors in the group and field environment at fixed redshift. The evolution of passive fraction in groups between  $z=0.4$  and  $z=0$  is consistent with a simple accretion model, in which galaxies are environmentally affected 3 Gyrs after falling into a  $\sim 10^{13} M_{\odot}$  group. This long timescale appears to be inconsistent with the need to transform galaxies quickly enough to ensure that star forming galaxies appear similar in both the group and field, as observed.

**Key words:** galaxies: clusters: general , galaxies: evolution

## 1 INTRODUCTION

The star formation history of a galaxy is a function of, at least, stellar mass, redshift and environment. In the local universe, a higher fraction of low mass galaxies are actively forming stars than more massive galaxies (Kauffmann et al. 2003; Brinchmann et al. 2004, B04). It has been known for some time that the star formation density of the universe has decreased by at least a factor of 10 in the last 8 or 10 Gyrs (Lilly et al. 1996; Madau et al. 1996; Hopkins 2004). There is growing evidence that this reduction with time is seen at all stellar masses (Gilbank et al. 2010b). Finally, at least in the local universe, the fraction of star forming galaxies in groups and clusters at fixed stellar mass is lower than

the general field (Kauffmann et al. 2004; Kimm et al. 2009). Untangling why and to what extent each of stellar mass, redshift and environment determine a galaxy’s properties is a fundamental goal of galaxy formation and evolution research. Ultimately, we hope to uncover the physical mechanisms responsible for each correlation.

The role of environment has been studied extensively by many groups (for recent reviews, see Boselli & Gavazzi 2006; Blanton & Moustakas 2009). Importantly, Weinmann et al. (2006) showed, by separating galaxies based on colour and specific star formation rate (based on  $H\alpha$ ), that the fraction of blue, star forming galaxies decreases with increasing halo mass at fixed luminosity. More recently, using UV derived star formation rates and the same group catalogue, Kimm et al. (2009) finds that the fraction of passive satellites increases with halo mass. These studies were largely

\* Email: s.l.mcgee@durham.ac.uk

focused on the fraction of passive galaxies, rather than the actual star formation rates.

Surprisingly, however, there is evidence that galaxies that are forming stars in groups have similar properties to those in the field; it is just that the fraction of those galaxies varies. For example, many authors (eg. Strateva et al. 2001; Baldry et al. 2004) have found that the local galaxy distribution is bimodal in colour, having a red and a blue peak. Balogh et al. (2004) finds that the peak of the red and blue galaxies change relative heights with environment at fixed luminosity. However, importantly, they find no significant difference in the location of the blue peak with environment (but see Wilman et al. 2010). Recently, Peng et al. (2010) found that the relationship between star formation rate and stellar mass was the same in the highest and lowest density quartile of galaxies. This implies the mechanism that transforms galaxies in dense environments must be rapid.

Strangulation, the process in which the hot gas halo surrounding a galaxy is stripped when it becomes a satellite in a large dark matter halo, is often thought to act over timescales of  $> 2$  Gyrs, seemingly in contradiction with the observational need for a rapid timescale (McCarthy et al. 2008). Therefore, a process that involves the ram pressure stripping of a galaxy's cold gas seems more viable. However, after correcting for the finite number of member galaxies, Balogh & McGee (2010) found that the intrinsic scatter between the red fractions in individual galaxy groups and clusters is remarkably small. When directly compared to models for how galaxies are accreted into groups and subsequently into clusters, this small scatter suggests that star formation must be truncated in haloes with mass  $\leq 10^{13} h^{-1} M_{\odot}$  (McGee et al. 2009). The efficiency of ram pressure stripping of cold gas in such low mass haloes is likely to be poor.

The next step is to look at the evolution of the key observational properties for further clues about the relevant mechanisms. It is difficult to obtain a large collection of unbiased and well sampled galaxy groups at high and intermediate redshift and thus the majority of the previous work has been based in the local Universe. To combat this, our collaboration, the Group Environment Evolution Collaboration (GEEC), has undertaken a detailed, multi-wavelength study of galaxy groups at intermediate redshift ( $0.3 < z < 0.55$ ) (Wilman et al. 2005). We have shown that these are truly galaxy groups — rather than clusters — as the group-sized velocity dispersions agree with stacked weak lensing and X-ray luminosities (Parker et al. 2005; Finoguenov et al. 2009). We have shown that the morphology-environment relation, using either visual or quantitative morphologies, while in place at  $z=0.4$ , grows stronger to  $z=0$  (McGee et al. 2008; Wilman et al. 2009). In addition, as in the local universe, the fraction of [OII] emitting galaxies, infrared excess galaxies or blue galaxies as a function of stellar mass is higher in the field than in the groups (Balogh et al. 2007; Wilman et al. 2008; Balogh et al. 2009).

[OII] emission can be effectively corrected to be a useful tracer of average star formation rates for large samples (Moustakas et al. 2006; Gilbank et al. 2010a). However, it is not clear that these corrections are effective for subsamples of galaxies, such as those that are affected by dense environments (Yan et al. 2006; Lemaux et al. 2010). In addition, to properly separate star forming from non-star forming galax-

ies, it is necessary to probe low star formation rates. It is difficult to attain this level of sensitivity with [OII], especially in low signal to noise spectra. In this paper, we use SED-fit star formation rates, that are driven by UV data from *GALEX*, and stellar masses, that are driven by *K* band data. This allows us to probe how star formation evolves as a function of environment and stellar mass since  $z=0.5$ .

In §2, we explain the two distinct surveys (GEEC and SDSS) used in the paper as well as the wide array of photometric and spectroscopic data used in both. We will also detail the new *GALEX* (§2.1.1) and CFHT Wircam K band (§2.1.2) observations that will be used to fit detailed spectral energy distributions. In §3, we explain the SED fits used in this paper including the fitting methodology and the sample of comparison stellar populations that are used to derive physical parameters. Finally, we simulate a sample of galaxies that allow tests of the robustness and accuracy with which we recover physical parameters (§3.4). In §4, we examine the environmental dependence of the SSFR -  $M_{\odot}$  diagram at both redshift epochs. In §5 we discuss the results and derive a plausible toy model for the truncation of star formation in group galaxies. Finally, in §6, we discuss our conclusions. In Appendix A, we make direct comparisons between our method of determining physical parameters and other methods from the literature.

Throughout this paper, we adopt a  $\Lambda$ CDM cosmology with the parameters;  $\Omega_m = 0.3$ ,  $\Omega_{\Lambda} = 0.7$  and  $h = H_0/(100 \text{ km s}^{-1} \text{ Mpc}^{-1}) = 0.75$ . Also, in this paper all magnitudes are stated within the AB magnitude system (Oke & Gunn 1983).

## 2 THE DATA

To achieve our goal of studying the evolution of the star formation properties of galaxies and their dependence on environment requires a sample of galaxies at two redshift epochs and deep UV observations. For our  $z=0.4$  sample, we use the sample of galaxies in the Group Environment Evolution Collaboration (GEEC) and deep *GALEX* observations made in Guest Observer mode. The low redshift sample of galaxies is derived from the Sloan Digital Sky Survey (SDSS) and its overlap with the *GALEX* Medium Imaging Survey (MIS). Below we detail each sample, as well as the group finding algorithms used.

### 2.1 GEEC survey

The GEEC survey was designed to provide highly complete and deep spectroscopy in the fields of galaxy groups selected from an earlier, sparsely sampled redshift survey – the Canadian Network for Observational Cosmology (CNOC2) Field Galaxy Redshift Survey. CNOC2 is a spectroscopic and photometric survey completed with the Multi-Object Spectroscopy (MOS) instrument at the 3.6m Canada France Hawaii telescope (CFHT) (Yee et al. 2000). The original survey targeted galaxies over four different patches of sky totaling about 1.5 square degrees. Spectroscopic redshifts of 6000 galaxies were obtained with an overall sampling rate of 48% to  $R_C=21.5$ . The survey used a band limiting filter that primarily limited successful redshifts to the range

$0.1 < z < 0.6$ , however, there was no colour pre-selection of targets.

Despite this relatively sparse sampling, Carlberg et al. (2001) were able to use a slightly modified friends of friends algorithm to define a sample of  $\sim 200$  galaxy groups. The only modification to the standard friends of friends algorithm, such as that described by Huchra & Geller (1982), is the requirement that the grouped galaxies are in a large scale overdensity. However, because of the sparse sampling of the survey, this step has no effect on the type of groups discovered.

These galaxy groups have been robustly characterised by weak lensing (Parker et al. 2005), mock catalogues (McGee et al. 2008), X-ray imaging (Finoguenov et al. 2009) and total stellar mass (Balogh et al. 2007). The mass estimates from all of these approaches agree well with the expected masses based on the average velocity dispersions of the groups. The mock catalogue analysis also found that the fraction of galaxies not associated with real galaxy groups was only 2.5% (ie. those not within  $0.5 h_{75}^{-1}$  Mpc of a  $> 10^{12} h^{-1} M_{\odot}$  halo).

The first step of the GEEC survey was presented in Wilman et al. (2005), in which the collaboration obtained follow-up spectroscopy in 20 regions, each centered on a Carlberg et al. group at  $0.3 < z < 0.55$ . This spectroscopy was obtained using the Multi-Object Spectroscopy Low Dispersion Survey Spectrograph (LDSS2) at the 6.5m Baade telescope at Las Campanas Observatory (LCO) in Chile. This targeting greatly increased the sampling in these 20 groups, as well as six other Carlberg et al. groups that were partially overlapping our targets on the sky. Thus, the completeness rose to  $\sim 78\%$  to a statistical limit of  $R_c=22$ . This was a half magnitude deeper than the original CNOC2 survey.

In this paper, we use data from both the targeted GEEC groups and the original Carlberg et al. groups, as well as making use of the full CNOC2 area from which to draw a comparison field sample. We correct for the incomplete sampling by adopting the weighting scheme described in Balogh et al. (2009). We apply weights to the galaxies based only the completeness as a function of  $R_c$  magnitude from the original CNOC2 images and their location inside or outside the LDSS2 follow-up regions. This weighting scheme allows a statistically complete sample to  $R_c = 22$  in the LDSS2 regions and to  $R_c = 21.5$  outside this region. Further  $1/V_{\max}$  weighting is applied to construct a statistically complete volume limited sample.

### 2.1.1 GALEX Observations

The Galaxy Evolution Explorer (*GALEX*) satellite is a NASA Small Explorer Class mission launched in 2003, which provides both imaging and grism capabilities in the ultraviolet (Martin et al. 2005; Morrissey et al. 2007). The *GALEX* satellite’s dichroic beamsplitter feeds both a Near Ultraviolet (NUV;  $\lambda_{\text{effective}} = 2271\text{\AA}$ ) and a Far Ultraviolet (FUV;  $\lambda_{\text{effective}} = 1528\text{\AA}$ ) detector, thereby providing simultaneous imaging in both bands over a very large, circular area ( $1.25$  diameter). The *GALEX* satellite has been revolutionizing galaxy formation and evolution studies since its launch by providing such wide field imaging in the ultraviolet. This is a particularly important waveband to enable a charac-

Patch	Central RA (J2000)	Central DEC (J2000)	NUV time (seconds)	FUV time (seconds)
2h	2:26:03.9	00:21:34	5843	5676
14h	14:49:38.1	09:10:58	11739	5115
21h	21:51:20.3	-05:31:27	8546	4682

**Table 1.** Details of the *GALEX* observations of the GEEC survey. Listed are the original CNOC2 patch name, the central right ascension (RA) and declination (DEC) of the *GALEX* pointings, as well as the combined FUV and NUV exposure time.

terization of the hot, massive and young stars that are indicative of recent star formation. Although, as we discuss, corrections must be made for both dust extinction and contributions from old stellar populations before robust star formation rates can be obtained.

We were awarded 9 orbits of *GALEX* observation time ( $\sim 13.5$  ks total) in Cycle 1 (PI: M. Balogh, ID: 037). This was intended to allow three orbits of observation time for each of three of the four CNOC2 patches. However, early in the *GALEX* mission, intermittent problems with the FUV detector caused some observations to be obtained with only the NUV images passing image quality tests. Thus, further observations were undertaken to insure that the full complement of FUV observing time was achieved. For this reason, the exposure time of the NUV images vary from 3 orbits per field (the 2 hour patch) to 6 orbits per field (the 14 hour patch). In Table 1, we detail the *GALEX* data of the three CNOC2 patches. Because of the L-shaped geometry of the original CNOC2 fields, the circular *GALEX* pointings do not cover the full patch. In this paper we restrict our analysis to galaxies within  $0.6$  of the center of the *GALEX* pointings.

We use the standard *GALEX* image reduction and calibrations obtained from the 2nd data release *GALEX* pipeline, as outlined in Morrissey et al. (2007). To provide a demonstration of the depth of our observations we present Figure 1, which shows the observed NUV-r color as a function of observed r magnitude in four different redshift bins. In this Figure, we have matched sources that are individually detected on the NUV images to the nearest GEEC galaxy within  $4''$ . The faintest NUV sources that are matched to GEEC galaxies have magnitudes of  $\sim 24.7$ , as shown by the black line in the figure. This figure is shown only as an illustration of the *GALEX* pipeline processed data. For the remainder of the GEEC analysis we use Point Spread Function (PSF)-matched magnitudes as detailed in §2.1.3.

### 2.1.2 CFHT Wircam K-band observations

In the 2009A observing season, we obtained observations in the K-band in the 14 and 21h fields using WIRCAM (Puget et al. 2004) on the Canadian France Hawaii Telescope (CFHT). Four pointings, each with 33 minutes of exposure time, were made in each of the two fields. Thus, each field had a region  $30' \times 30'$  mapped out. Each pointing was divided into 80 exposures of 25 seconds each, and was dithered in a 5 point pattern to fill in the chip gaps. The

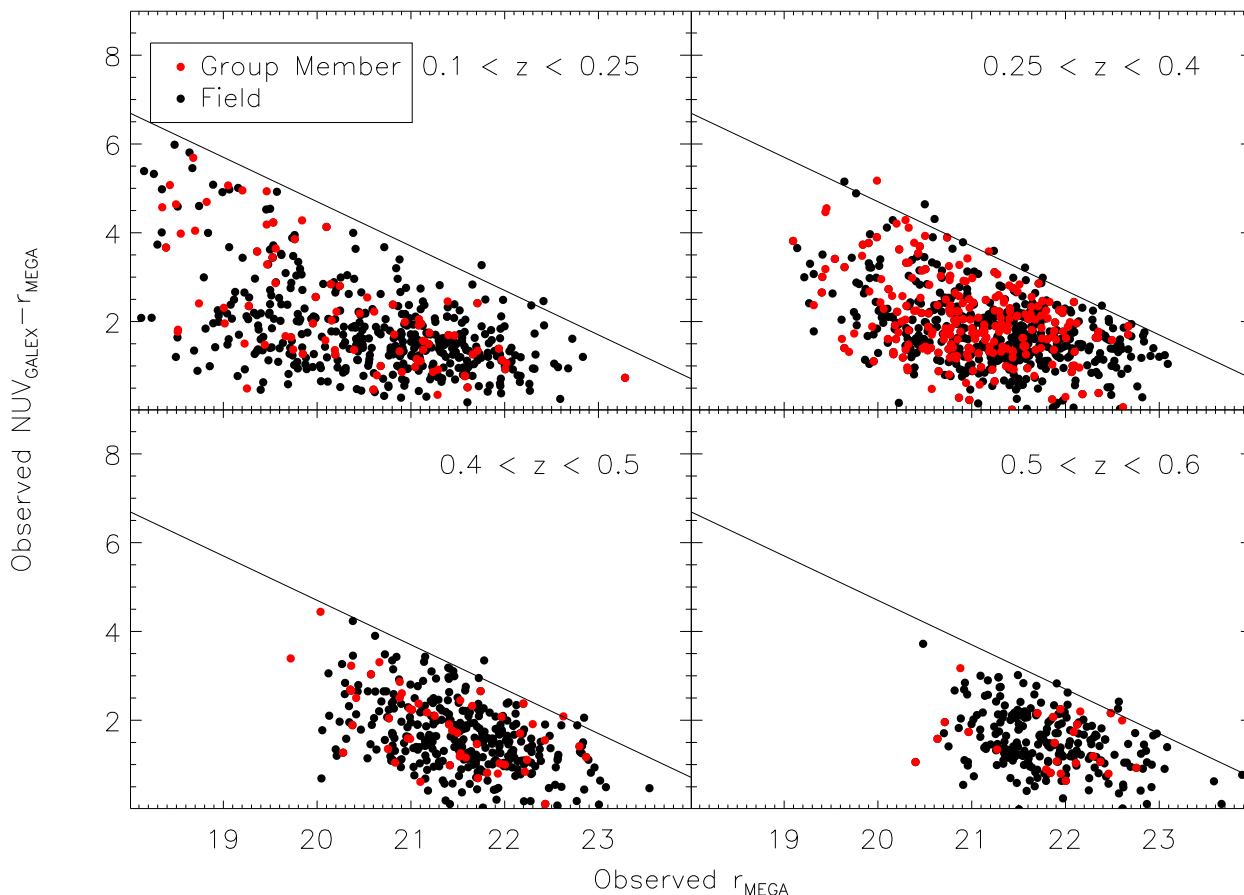


**Figure 1.** Observed colour-magnitude diagram in the *GALEX* NUV and CFHT Megacam *r* bands in four redshift bins within the GEEC survey. The black line is at  $\text{NUV}=24.7$ , which illustrates the limit of the faintest sources detected in the *GALEX* images. The red points are group members while the black points are field galaxies.

data were then reduced and processed by the Elixir<sup>1</sup> and Terapix<sup>2</sup> pipelines.

### 2.1.3 PSF matching and Photometry

There are at least two approaches to measuring accurate colours for sources in images with different resolution. One approach is to make a detailed model of the source in each image with the intent on measuring its "total" magnitude in each band. This is the approach we will use with the low redshift data, largely because of the availability of well understood "model" magnitudes in the SDSS. However, in the GEEC survey we take the second approach: using aperture-based photometry after adjusting the images to have the same PSF.

The original photometry of the CNOC2 survey was not accurate enough to allow detailed SED-fitting. In Balogh et al. (2009), we presented the results of an extensive campaign to obtain new optical and near-infrared photometry. In this paper, we follow the same general scheme

for making photometric measurements. While we briefly discuss this scheme below, we refer the reader to Balogh et al. (2009) for the full details.

The original GEEC object detection was done on a combined  $R(\text{CFH12K})$  and  $r(\text{Megacam})$  'super' image for each of the CNOC2 patches. This image was used for detection as it allowed for the greatest depth and coverage, while closely resembling the original  $R_C$  band used in sample selection. We use this 'super' image only for object detection, and use each filter (including  $r$  and  $R$ ) separately for the photometry. All the photometric images, including the *GALEX* NUV, FUV and Wircam K-band images, were aligned to the corresponding super image using SWARP (Bertin et al. 2002) after assuring that the astrometric alignment was correct. In Table 2, we list each of the instruments and filters used in the paper. We also list the fraction of galaxies in the GEEC sample that are covered by each filter. Notice that this simply measures the fraction of galaxies within the footprint of the data, rather than the fraction detected.

The *GALEX* images have the largest PSF of any of our images ( $\sim 4.7''$ ), so we convolve each of our images with a Gaussian kernel appropriate to obtain a PSF of  $4.7''$ . We then use SEXTRACTOR v2.5 (Bertin & Arnouts 1996) in two-image mode on each image, with the unconvolved 'su-

<sup>1</sup> <http://www.cfht.hawaii.edu/Instruments/Elixir/>

<sup>2</sup> <http://terapix.iap.fr/>

per'  $r$  image as the detection image. The photometry is then measured within  $10''$  apertures, thus ensuring that we obtain PSF-matched colors for all the wavebands. Total magnitudes are derived by computing the CFH12K  $R$  or Megacam  $r$  SExtractor MAG\_AUTO parameter in the unconvolved image and then using the appropriate aperture color. It is this photometry we use for the rest of the GEEC analysis.

Measuring photometry in large apertures could introduce biases due to crowding from other galaxies. We test how often this occurs by examining the difference in implied total magnitude in the optical wavebands when using  $3''$  apertures in the unconvolved image to that implied using  $10''$  apertures in the convolved image. Each of the optical wavebands provide a consistent picture, that approximately 7% of galaxies are affected by crowding. For instance, in the Megacam I band, we find that 7.3% of the galaxies have implied total magnitudes which differ by more than 0.2 mags. Visual inspection of these galaxies confirm that the errors are due to crowding by nearby galaxies. However, the fraction of the group galaxies which suffer from crowding measured in this way (6.9%) is essentially equivalent to field galaxy fraction (7.4%). The removal of these galaxies from the sample do not affect the results, and we leave them in the sample for completeness.

We have assumed that the *GALEX* PSF is a Gaussian profile with a  $4.7''$  FWHM. However, detailed measurements have shown that the PSF varies from  $4.2''$  to  $5.3''$  (FWHM) in the FUV and NUV channels, respectively (Morrissey et al. 2007). We examine how these refinements affect our photometry by examining the Megacam  $u$  data. The  $u$  data is perhaps the most sensitive to proper PSF matching to the *GALEX* data as the NUV- $u$  color is a measure of the dust attenuation at these redshifts. We have convolved the  $u$  data with a  $4.2''$  Gaussian and a  $5.3''$  Gaussian (FWHM). The dispersion in  $u$  magnitude implied from comparing these two images is only  $\Delta\text{mag} \sim 0.017$ , which is smaller than our applied zeropoint uncertainty. The *GALEX* PSF is also not strictly Gaussian, although the largest variations are in the wings, which has little effect on our data. These variations from gaussianity are also a function of position on the detector. We avoid the extreme effects of non-gaussianity by restricting to the central 0.6 degrees of the field of view.

We do not apply Galactic extinction corrections directly to the photometry. We want to avoid adding extinction corrections to negative fluxes, which occasionally result from a non-detection. Instead, we apply a correction to each of the population synthesis models based on the measured extinction from Schlegel et al. (1998) for each patch of the survey. This essentially adds the reddening effect of Galactic extinction to the models, allowing a direct comparison with the photometry.

We restrict the analysis in this paper to galaxies with  $r < 22$  within the fields with follow-up spectroscopy and to  $r < 21.5$  within the rest of the survey. This has been shown to allow an unbiased statistical sample with no colour dependence to be generated (Yee et al. 2000; Wilman et al. 2005). Due to this restriction, the majority of our galaxies are well detected in all the photometric bands that have coverage in the area.

The SExtractor magnitude errors are computed in the standard way, using the distribution of background

Instrument	Filter	Fraction covered
GALEX	FUV	1.
	NUV	1.
CFH12K	$B$	0.596
	$V$	0.591
	$R$	0.594
	$I$	0.626
Megacam	$u$	0.797
	$g$	0.794
	$r$	0.789
	$i$	0.561
	$z$	0.787
INGRID	$K_s$	0.112
SOFI	$K_s$	0.210
WIRCAM	$K$	0.543

**Table 2.** The filters used for SED fitting of GEEC galaxies in the *GALEX* sample. The instrument used for the photometry is listed along with the fraction of galaxies which are covered by each given waveband. 96.2% of all GEEC galaxies in the *GALEX* sample have either  $R$  or  $r$  band coverage, while 71.2 % have  $K$  or  $K_s$  band coverage.

noise (Bertin & Arnouts 1996). However, when comparing to SEDs it is important that these errors are not underestimated, and thereby disfavor models which are good fits. To avoid this, we compute a photometric error correction by examining the standard deviation of the magnitude dependent difference between observations of the same galaxy in two similar filters. At each half magnitude, we scale the average error implied by SExtractor to equal that implied using similar filters. We assume that the scaling factor is due to both filters equally. This enables us to estimate, for each filter, a photometric error correction that depends only on observed magnitude, and this is used for all galaxies in the sample. This procedure will slightly overestimate the uncertainty because of real variation in galaxy types, which causes an intrinsic variation in the color. However, that variation is expected to be on the order of 0.05 magnitudes (Fukugita et al. 1995). We also add zeropoint errors of 0.05 magnitudes to each of the filters in quadrature, except for NUV, INGRID and SOFI data, which we have zeropoint errors of 0.03, 0.17 and 0.1 mags, respectively.

In order to maintain the unbiased properties of the survey, we restrict our discussion to galaxy groups that were pre-selected from the sample of Carlberg et al. (2001). However, we do redefine the galaxy groups using the Wilman et al. (2005) spectroscopy. We follow the redefinition scheme described extensively in McGee et al. (2008) and based on Wilman et al. (2005). We define galaxy group members as those that are within  $500 h^{-1}$  kpc of the luminosity weighted group centre and have a line of sight velocity within two times the velocity dispersion of the group redshift. Using this method, our final sample of 2347 galaxies between  $z=0.3$  and  $z=0.55$  contains 335 group galaxies. Figure 2 shows the measured velocity dispersion of our galaxy groups as a function of redshift. For clarity, we have omitted velocity dispersion uncertainties, which are typically  $\pm 100$  km/s, or upper limits, which arise in a few cases when the velocity errors are larger than the velocity dispersion. Full details of the velocity dispersion calculations are in Wilman et al. (2005).

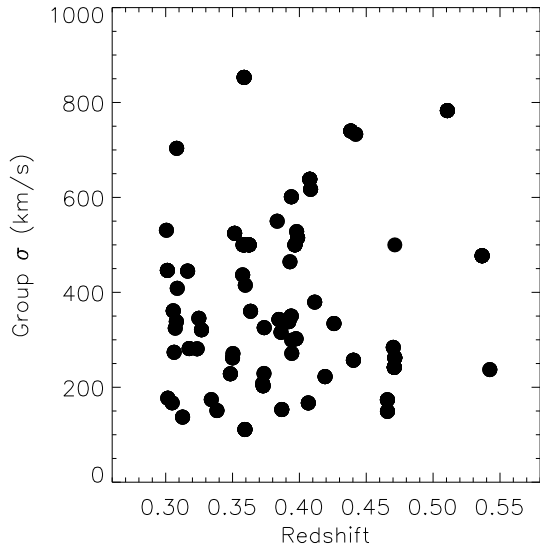


**Figure 2.** The velocity dispersion as a function of redshift for GEEC galaxy groups in our three fields with *GALEX* data. We restrict our sample to the groups shown, which lie between  $z=0.3$  and  $z=0.55$ . The typically error in the velocity dispersion is  $\pm 100$  km/s.

In this paper, we call galaxies in our groups to be ‘group galaxies’ and we define the ‘field’ sample to be all other galaxies. The field sample is not an ‘isolated’ sample, as it will have many groups contained within it that are undetected by the sparse CNOC2 redshift survey. Indeed, we have shown in a previous paper (McGee et al. 2008), that the ‘field’ sample is very close to a global sample of galaxies and thereby contains close to the universal fraction of group galaxies within it.

## 2.2 SDSS survey

The Sloan Digital Sky Survey (SDSS) is a five colour (*ugriz*) photometric and spectroscopic survey (York et al. 2000). In this paper, we make use of the Data Release 6 (DR6), which contains over 790,000 galaxy spectra within approximately  $7425 \text{ deg}^2$  (Adelman-McCarthy et al. 2008). We restrict our analysis to only galaxies within the main galaxy sample, which targets almost all galaxies with  $r \leq 17.77$  (Strauss et al. 2002). Some galaxies are left unobserved because of the finite size of the fiber optic spectra plugs, which does not allow two galaxies to be observed when they are within  $55''$  of each other (Blanton et al. 2003).

We use the *ugriz* MODEL MAG, which is designed to give the most accurate galaxy colour while still being close to a total magnitude (Stoughton et al. 2002). The SDSS photometry has zeropoint calibration errors of approximately 0.01 mag in *g,r*, and *i*, 0.02 mag in the *z* band and 0.03 in *u* (Ivezić et al. 2004).

### 2.2.1 GALEX data

The *GALEX* Medium Imaging survey (MIS) was designed to provide single orbit ( $\sim 1500$  second exposure) of approxi-

mately 1000 square degrees of the SDSS (Martin et al. 2005; Morrissey et al. 2007). We use 1017 tiles of the MIS that were released to the public via the 3rd General Release. We retain only objects within the central  $0^\circ.6$  of each *GALEX* pointing, and resolve overlapping observations by keeping the one nearest the pointing center. The photometry from the *GALEX* pipeline is computed using SExtractor in two image mode. In the pipeline, a detection image is created by dividing a background-subtracted data image to a corresponding detection threshold map. SExtractor uses any pixel in the ratio with values greater than one as possible detections, and measures the corresponding photometry using a background subtracted image.

We follow the work of Budavári et al. (2009), who showed that an effective matching of SDSS galaxies and *GALEX* sources could be made by matching to the nearest source within  $4''$ . We use all galaxies within the main galaxy sample of the SDSS as our starting point. We reduce this sample to those galaxies within  $0^\circ.6$  of a MIS tile and subsequently match to NUV/FUV sources from the *GALEX* SExtractor catalogs. We use the MAG\_AUTO photometry, which is close to a total magnitude. We do not attempt to explicitly match the PSF of this photometry with the SDSS photometry as we have done for the UV-optical data of the GEEC sample. Our use of SDSS MODEL MAG assures that we are measuring total magnitudes in both regimes, and thus PSF matching is of less importance. The use of fixed apertures such as was done in the GEEC sample would introduce significant redshift bias due to the factor of 12 difference in physical size of an arcsec throughout the low redshift sample. Further, the resolved galaxies of the low redshift sample make the PSF becomes less critical. The final sample of galaxies in the SDSS/*GALEX* overlap between  $z=0.01$  and  $z=0.15$  is 49663. 87% of these galaxies are detected at the  $3\text{-}\sigma$  level in *NUV* and 79% at the same level in *FUV*.

### 2.2.2 Group finding

In an attempt to compare the redshift evolution of group properties as fairly as possible, the primary goal of our low redshift group finder is to reproduce the selection of our GEEC groups. The method is very similar to the method used and described in McGee et al. (2008) for low redshift groups.

GEEC groups were selected from a shallower and more sparsely sampled redshift survey than the SDSS. Thus, we apply two filters to the SDSS galaxies before applying the group finding algorithm. First, we apply the same absolute magnitude cut as the original CNOC2 group finder,  $M_R = -18.5$  with an applied evolution correction of 1 mag per unit redshift. Secondly, we randomly remove half of the remaining galaxies to replicate the completeness of the CNOC2 redshift survey.

For all of the remaining galaxies, the local density was calculated by counting the galaxies within a cylinder of  $0.33 h_{75}^{-1} \text{ Mpc}$  and  $\pm 6.67 h_{75}^{-1} \text{ Mpc}$  line of sight depth centered on it. If the galaxy has fewer than three neighbours then the cylinder is expanded in every direction by 1.5 and the neighbours recounted. The galaxy is only available to become a grouped galaxy if it has a higher density than the background.

The groups are then compiled by beginning at the highest density galaxy and adding all the galaxies within its cylinder. Next all the galaxies in each of the cylinders centered on those galaxies are added. This continues until no more galaxies are added to the “proto-group”. Members of this group are then used to calculate the geometric center, redshift and velocity dispersion ( $\sigma_v$ ). Using these quantities as starting points, galaxies are added or removed iteratively that within  $1.5R_{200}$ , where  $R_{200} = \sqrt{3}\sigma_v/[10H(z)]$ , and three times the velocity dispersion. This process is repeated until convergence.

Using this sample of groups, we now add in all the galaxies that were randomly removed to reduce the completeness. This allows us to emulate the GEEC follow-up of the Carlberg et al groups. The geometric center, redshift and velocity dispersions were again re-computed, now using all available galaxies. To avoid edge effects, we run the group finder on the entire SDSS DR6 main galaxy sample, and then subsequently restrict ourselves to groups within the SDSS/*GALEX* overlap region.

As in the GEEC sample, we call all the galaxies which reside in our groups using this method ‘group galaxies’ and describe the rest of the SDSS sample as ‘field galaxies’. But again, due to incomplete sampling, the ‘field’ sample has close to the universal value of galaxy groups.

This process of finding groups has been shown in McGee et al. (2008) to reproduce a similar halo mass distribution for both GEEC and SDSS galaxy groups when simulated in mock catalogs. While it is outside the scope of this paper, in an upcoming work, we will further examine the group properties at both epochs, including the concentrations and degree of Gaussianity in velocity distributions (Hou et al., *in prep.*). The CNOC2 survey (on which GEEC is based) and the SDSS survey select galaxies only based on  $r$  band, with no color selection. The similarity in selection and group halo mass function suggests that the GEEC and SDSS samples can be fairly compared without a strong bias. However, we should remember that the two redshift epochs are the result of different surveys and subtle systematic biases may remain. To minimize the effect of this, we focus principally on comparing the group and field behavior at a given epoch, and analyse how these relative differences change between epochs.

### 3 FITTING SPECTRAL ENERGY DISTRIBUTIONS

UV photometry, while extremely useful for measuring young stars, is sensitive to attenuation from dust. Early studies analysing UV photometry from star bursting and rapidly star forming galaxies found that a reasonable dust correction could be made by assuming that the galaxy’s spectral slope in the UV was proportional to the dust attenuation (Meurer et al. 1995; Calzetti et al. 2000). However, when ultra-violet light was observed in normal star forming galaxies, and even relatively quiescent galaxies, it was found that there is no universal relation between the UV slope and UV dust attenuation (Bell 2002; Cortese et al. 2008). In effect, the UV slope overestimates dust attenuation for galaxies with significant old populations. This is particularly impor-

tant when studying massive galaxies and those in groups because of their expected old populations.

To overcome these problems, we use all the available photometry (optical, near-infrared and UV data), to systematically compare against a sample of models created from the population synthesis code of Bruzual & Charlot (2003). This specific method we follow is that of Salim et al. (2007), who have earlier used a similar SDSS/*GALEX* overlap sample.

The general technique involves using a sample of template SEDs with known galaxy parameters. The templates are fit to the observational photometry and the galaxy parameters of the best fit model, or the weighted likelihood of all models, are adopted as the parameters of the observed galaxy. Below we discuss the template SEDs that we create using stellar population synthesis (§3.1) and then discuss the detailed methodology we use to find the best fitting parameters (§3.2).

#### 3.1 Model Stellar Populations

All our galaxy templates are created using Bruzual & Charlot (2003) models with a Chabrier initial mass function (Chabrier 2003), assuming a lower (and upper) IMF mass cutoff of 0.1 (100)  $M_{\odot}$ . These templates use the Padova 1994 evolutionary tracks (Alongi et al. 1993; Bressan et al. 1993; Fagotto et al. 1994a,b), while the stellar spectra are drawn from the BaSeL 3.1 (Bessell et al. 1989, 1991; Allard & Hauschildt 1995) and STELIB (Le Borgne et al. 2003) spectral libraries.

We follow the galaxy parameter ranges used and justified by Salim et al. (2007). The model spectra are produced by randomly selecting values for a set of variables that control the model galaxy’s age, metallicity, star formation history and dust obscuration. In particular, the age of the galaxy is randomly selected from a uniform logarithmic distribution between 0.1 Gyr and the age of the Universe at the epoch of observation. The metallicity is uniformly spaced between  $Z=0.005Z_{\odot}$  and  $2.5Z_{\odot}$ , where the canonical solar metallicity is  $Z_{\odot}=0.02$ . 96% of the model galaxies have metallicities between  $Z=0.1-2.5Z_{\odot}$ .

We assume that the star formation histories of these galaxies have a backbone of exponentially declining star formation rates, and superimposed onto this backbone history are star formation bursts. In particular, the backbone rates are randomly chosen with a uniform distribution in  $\gamma$  ( $SFR \propto \exp(-\gamma t)$ ), where  $\gamma$  is  $0 \leq \gamma \leq 1 \text{ Gyr}^{-1}$ . On this backbone, we allow bursts that last some time randomly distributed in duration between 30 and 300 Myr. The strength of the bursts are also randomly chosen so that during the lifetime of the burst they produce between 0.03 and 4 times the stellar mass the galaxy had at the onset of the burst. These bursts are randomly assigned so that there is a 25% chance a galaxy will undergo at least one burst in a given Gyr. Each Gyr is independent, and thus many galaxies go longer than 4 Gyrs without a burst. If the galaxy has formed more recently than a Gyr, then the chance of it having a burst is prorated. This is the same burst frequency and strength adopted by Kauffmann et al. (2003) after examining the burst diagnostic plane of  $D_n(4000)$ - $H\delta$ , and subsequently adopted by Salim et al. (2007). Note that, given the length and frequency of bursts, only  $\sim 4\%$  of model galaxies

are undergoing a burst at any one time. This is similar to the 5% duty cycle of galaxies exceeding 0.6 dex from the SFR sequence found by Noeske et al. (2007).

We adopt the simple two-component dust model of Charlot & Fall (2000). In this model, young stars are shrouded in the dust associated with their birth, which has an associated optical depth to the observer of  $\tau_v$ . After birth these young stars gradually disrupt and or dissipate their dust clouds. This is modelled by assuming that only some fraction,  $\mu_v$  of the original optical depth remains 10 Myr after the stars birth. The  $\tau_v$  is drawn from a distribution that peaks at 1.2 magnitudes of attenuation and runs from 0 to 6 mags. The  $\mu_v$  value runs from 0.1 to 1, peaking at 0.3.

We then create model magnitudes by convolving the Bruzual & Charlot (2003) resultant spectra with filter curves of *GALEX* NUV and FUV bands as well as the SDSS *ugriz* for the low redshift sample. The model magnitude catalogs are generated at each 0.03 redshift interval from  $z=0.02$  to  $z=0.20$ . When comparing these model catalogs to actual data, we interpolate between the nearest redshift intervals for each template to simulate the proper k-corrections. Finally, the distance modulus is applied to simulate that observed galaxy redshift. In the GEEC sample, we convolve the spectra with the expected transmission of *GALEX* NUV and FUV, CFH12K *BVRI*, Megacam *griz*, Wircam *K<sub>s</sub>*, and 2MASS *K*. We use the 2MASS filter because both the IN-GRID and SOFI *K* band data were calibrated to give magnitudes on the 2MASS system. We generate catalogs every 0.05 redshift interval from  $z=0.3$  to  $z=0.55$  and apply interpolated k-corrections and distance moduli.

### 3.2 Fitting Methodology

The set of model galaxies we have generated by randomly sampling the allowed parameter space acts as a Bayesian prior to the physical galaxy parameters. Our goal is to find a resultant probability distribution function (PDF) for each parameter and for each observed galaxy. For a given observed galaxy, we find the scale factor,  $a_i$ , that gives the minimum  $\chi_i^2$  for each model galaxy,  $i$ , in Equation 1.

$$\chi_i^2 = \sum_X \left( \frac{F_{\text{obs},X} - a_i F_{\text{mod},i,X}}{\sigma(F_{\text{obs},X})} \right)^2 \quad (1)$$

In which,  $X$  represents the sum over the 7 bands of low redshift photometry and the 12 bands of GEEC photometry.  $F_{\text{obs},X}$  then represents the flux in the  $X$ th band of the observed galaxy, while,  $F_{\text{mod},i,X}$  is the  $X$ th band flux of the given model galaxy.  $\sigma(F_{\text{obs},X})$  is the error of flux in the  $X$ th observed band.

We use all available photometric bands for each galaxy. The only exception arises with *GALEX* NUV data, and at low redshift, FUV. These are unique bands for two reasons. First, it is these bands that largely drive our star formation rates and are thus especially important. Secondly, these are the only bands for which there are a significant number of non-detections. Therefore, for galaxies that are not detected in the original NUV or FUV imaging, we restrict the space of models to have NUV-r or FUV-r colours redder than the observed limits. This effectively puts more weight on the NUV and FUV points given their importance in probing

the SFR. The non-detections, which make up  $\sim 20\%$  of GEEC and  $\sim 13\%$  of SDSS galaxies, are only in the region of 'non-starforming' galaxies, and is largely the cause of our slight 'overestimate' of the SFR in passive galaxies, as shown in §3.4.

While the SDSS spectroscopic sample is derived from the  $r$  band photometry, the remaining bands of photometry are sufficiently deep that accurate colors are obtained for all of the galaxies drawn the main galaxy sample in our redshift range of interest. Similarly, with the GEEC photometry, except for the  $z$  band data, all galaxies are brighter than the expected limits. However, at the faint end, the  $z$  band photometric errors become large enough to encompass the models which are beyond the photometric limit, so we take no explicit action for these.

The  $\chi^2$  value of each model galaxy is then used to define a weight,  $\exp(-\chi_i^2/2)$  for that model in fitting the given observed galaxy. The galaxy parameters of that model are then all given the weight,  $w_i$ . Once all models have been assigned a weight, each galaxy parameter has a PDF constructed by compounding the associated weights at each parameter value range. We then obtain the parameter values that correspond to the median of the PDF. Also, we obtain an approximation to  $1\sigma$  error bars by using 1/4 of the 2.5-97.5 percentile range, and we will quote typical measurement errors based on this.

The star formation histories we use in the models of Bruzual and Charlot have a time resolution of  $10^7$  years. Therefore, the final galaxy parameters at any given epoch are representative only of the galaxy within the last  $10^7$  years. However, UV star formation rates are sensitive to any star formation within the last 100 Myrs because this is the lifetime of the massive stars that produce UV emission. In other words, a burst of star formation will shine in the UV for 100 Myrs. Accordingly, we average the final 100 Myrs of any simulated Bruzual Charlot galaxy to produce a parameter that the UV is tracing. Thus, when we refer to star formation rates produced by this SED fitting, we are referring to the average star formation rate within the past 100 Myrs.

### 3.3 Dust enshrouded star formation

As we show in Appendix A, the SED-fit star formation rates agree very well with the rates inferred from star forming galaxies using dust corrected  $H\alpha$  emission. However, the possibility exists that some star forming galaxies could be so optically thick that they would not emit significantly in  $H\alpha$  or UV. Using star formation rates inferred from UV/optical photometry like ours and comparing to mid-infrared star formation indicators, Salim et al. (2009) found that indeed most of the star forming galaxies were not optically thick.

To obtain a star formation rate from mid-infrared photometry, such as that taken at  $24 \mu\text{m}$  by the Spitzer Space Telescope (Werner et al. 2004), a correction is made to obtain the total infrared emission emitted by the galaxy. In the standard manner, this correction is found by assuming a model, usually empirical, which constrains the SED in the infrared. There are a variety of models available and Salim et al. (2009) found that the UV SED fit star formation rates could reproduce the mid-IR derived star formation rates to within a factor of 2 using the UV/optical photom-



etry alone when using the models of Chary & Elbaz (2001) and Dale & Helou (2002). However, when using the more recent templates of Rieke et al. (2009), the UV/optical photometry did not accurately reproduce the dust measured SFR in the sense that Rieke et al method gave higher star formation rates. We present analysis of 24  $\mu\text{m}$  photometry for GEEC galaxies in Tyler et al. (submitted), which uses the Rieke et al. (2009) templates. We show there that the amount of dust enshrouded star formation per galaxy is similar in the groups and in the field. Since the Rieke et al. templates give higher amounts of obscured star formation than the Chary & Elbaz (2001) or Dale & Helou (2002) templates, assuming either type of template makes it unlikely that we are missing a significant population of optically thick star formation that only exists in one environment. Indeed, Tran et al. (2009), using the templates of Dale & Helou (2002), found that a comparable fraction of  $\text{SFR} > 3 M_{\odot}/\text{yr}$  galaxies were found in the group environment and in the field environment.

### 3.4 Simulating galaxy samples

As will be introduced in § 4.1, the galaxy parameters we use in this paper are principally the specific star formation rate (SSFR; the star formation rate divided by the stellar mass) and the stellar mass. In Appendix A, we have attempted to quantify the accuracy of these galaxy parameters by comparing them to parameters obtained using other, largely independent methods. However, this approach is not fully satisfactory, because the parameters can only be tested for limited cases, ie.  $\text{H}\alpha$  measurements provided only constraints on the low redshift, star forming galaxies. We do not have a similar test available for the GEEC data. Thus, in this section, we create a mock sample of observations of galaxies for which we know the "true" SSFR and stellar mass, which allows us to establish the legitimacy of our fitting procedure.

For each survey, we create a sample of 100,000 mock galaxies that are drawn from the same distribution of dust, metallicity, age and star formation parameters from which the fitting templates were drawn, as described in §3.1. However, while the mock galaxies and fitting templates are drawn from the same distribution, no single mock galaxy has the exact same parameters as any one of the fitting templates. The mock galaxies are normalized to have stellar masses between  $10^8$  and  $10^{12} M_{\odot}$ , and are then placed at  $z=0.08$  (SDSS mock galaxies) and  $z=0.4$  (GEEC mock galaxies). Mock observations are then created using the 7 filters of the SDSS sample and the 12 filters of the GEEC sample. For each mock galaxy, the photometry in each band is given a random Gaussian error consistent with the expectations of that bands measurement and zeropoint errors. In the GEEC sample, we also simulate the heterogeneous nature of the waveband coverage by removing observations in order to reproduce a sample with the same fraction of coverage in each band. However, as in the real method, we always have a minimum of 4 filters of coverage, including *GALEX* NUV and at least one band at *r* or redder. Crucially, we also simulate the depth of the *GALEX* NUV and FUV data. When the mock NUV or FUV observation is beyond the magnitude limit of our real observations, we restrict to fitting only models with an NUV-*R* and FUV-*R*

color greater than the color at the NUV and FUV observation limit.

In Figure 3, we present the stellar mass parameters that result from SED-fitting the mock set of simulated galaxies in both surveys. We show the difference between the "true" stellar mass and those obtained by SED fitting the mock observations as a function of the SED masses. The fitting recovers very well the true stellar mass, with only a nominal systematic offset and no mass dependent deviations in the adequacy of the recovery. Note that the  $z=0.4$  sample has a smaller scatter ( $\sigma = 0.081$  dex) than the  $z=0.08$  sample ( $\sigma = 0.129$  dex). This is likely because we restrict the age of galaxies in the models to be less than the age of the Universe at that epoch, which means that the  $z=0.4$  sample has less cosmic time for wide variations in star formation histories.

In Figure 4, we show the SSFR results produced from SED fitting the mock galaxies. Unlike the stellar mass comparison, we see a systematic deviation from the true SSFR that depends on the SSFR. At the star-forming end, greater than  $\log_{10}(\text{SSFR}) = -10.75$  at  $z=0.08$  and  $\log_{10}(\text{SSFR}) = -11$  at  $z=0.4$ , the SSFR is reproduced correctly with small scatter ( $\sim 0.25$  dex at low redshift and  $\sim 0.2$  dex at  $z = 0.4$ ). However, below these points, the SED fit SSFR seems to systematically overestimate the true SSFR by  $\leq 0.3$  dex. This behavior is a direct result of the depth of the *GALEX* NUV data. As we have mentioned, when the NUV magnitude is beyond our completeness, we simply restrict model space to those models that have (*NUV* - *R*) colours redder than that. Thus, the SSFR is essentially an average of the remaining models, which leads to a slight overestimate of the SSFR. This is indicative that our priors for low star formation rate galaxies are not correct. However, in this paper we restrict ourselves to analysis only of the high star formation rate galaxies and the fraction of these; thus, our slight overestimate of the SSFR has no impact for the present analysis and we do not try to develop more rigorous priors. Also, notice in Figure 4 that there is a population of galaxies undergoing an intense burst of star formation and thus have very high SSFRs ( $\sim 10^{-8} \text{ yr}^{-1}$ ).

Our mock sample fitting has led to two important points. First, as also evidenced by our comparisons with published stellar masses in §A, we are able to accurately recover stellar masses to the level of  $\sigma = 0.2$  dex over the full range of mass within the constraints of the models. Second, we have shown that we can recover SSFR for star forming galaxies, but that we may be overestimating the SSFRs of non-star forming galaxies. This is an important point, since the Brinchmann et al. (2004, B04) star formation rates did not allow us to estimate our accuracy at low SFR. With these findings in mind, in this paper, we avoid making a detailed analysis of the rates of low star forming galaxies and instead set a threshold for the division of active and passive galaxies at  $\log_{10}(\text{SSFR}) = -11$ , essentially lumping all passive galaxies together.

## 4 RESULTS

### 4.1 SSFR- $M_{\odot}$ plane

The star formation rate of a galaxy is a key indicator of galaxy evolution, and for active galaxies there is a strong

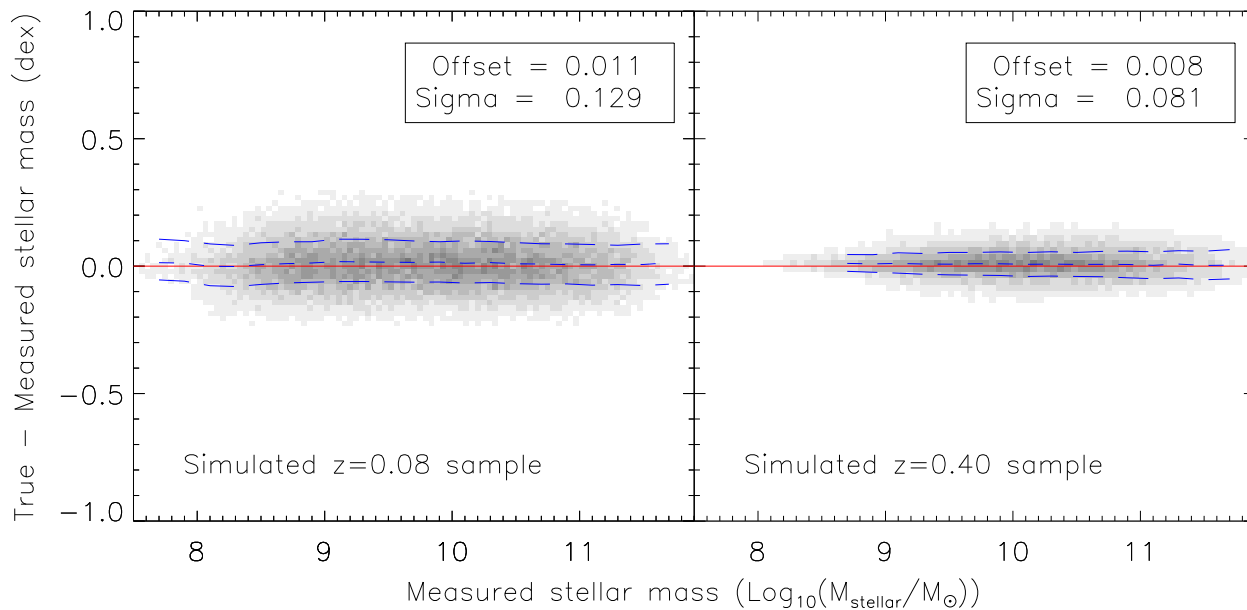


**Figure 3.** Comparison between the “true” stellar masses of a mock set of simulated galaxies and the SED fit stellar mass of the mock galaxies. This is shown for both the  $z=0.08$  simulated sample (left panel) and the  $z=0.4$  sample (right panel). The solid red line in both plots shows where the difference in measurements is 0. The blue, central dotted line represents the running median of the offset, while the two blue, dashed lines show the  $1\sigma$  limits.

correlation between star formation and stellar mass. Many authors, (eg. Kennicutt 1983; Scalo 1986; Brinchmann et al. 2004), have thus examined the specific star formation rate (SSFR) which is defined as the star formation rate normalized by the total stellar mass of the galaxy:

$$\text{SSFR} \equiv \frac{\text{SFR}}{M_{\text{stellar}}} \quad (2)$$

This is a useful approach because it quantifies the current SFR with respect to the past SFR (Kennicutt et al. 1994). For instance, a value of SSFR of  $10^{-9} \text{ yr}^{-1}$  means that if the galaxy maintains its current SFR for  $10^9 \text{ yr}$ , then it will double its stellar mass. SSFR can then easily be converted into a “birthrate”,  $b$ , defined as  $b = \text{SSFR} \times t$ , where  $t$  is the age of the universe. A value of  $b$  greater than 1 means the galaxy is forming stars faster than it has in the past. Of course, this is an approximation, as the galaxy may have been forming stars for only a fraction of the age of the universe, or had a significant amount of the formed stellar mass returned to the ISM.

It is with this intuition that we present Figure 5, which shows the SSFR as a function of the galaxy stellar mass for galaxies in the SDSS sample. We have two panels: one showing the field galaxies, and one showing the group members. It should be noted that the points each represent individual galaxies, but that the galaxies have not been weighted by  $1/V_{\text{max}}$ . Thus, especially galaxies in the bottom left corner (those of low mass and SSFR), are systematically under-represented. However, when defining passive fractions or other quantities we always account for these weights.

Examining this figure, it is apparent that galaxies appear bimodal in the SSFR- $M_{\odot}$  plane. They tend to cluster

as part of either a group of passive galaxies at  $\text{SSFR} \sim 10^{-12}$ , or a group of star forming galaxies at  $\text{SSFR} \sim 10^{-10}$ . This behavior is obvious in both the group and field galaxies. The galaxies clustered at  $\sim 10^{-10}$  has been called by other authors the “main sequence of star-forming galaxies” (Noeske et al. 2007). These galaxies have a birthrate,  $b$ , of approximately 1, which could suggest that they have been forming stars at about this rate for their lifetime.

It is important to remember that, as shown in §3.4, the low SSFR rates were actually slight overestimates, meaning that the cluster of points at  $\text{SSFR} \sim 10^{-12}$  is unlikely to be caused by systematically low SSFR measurements. In other words, this ‘main sequence’ is not due to an insensitivity to star formation rates just underneath the sequence. This is a crucial point as the work of Noeske et al. (2007) was based principally on emission lines, which are relatively insensitive to low star formation rates. We stress that because our star formation rates are based on SED-fitting, they are complete as a function of stellar mass, with no selection on the star formation rate. Thus, similar to the behaviour seen in galaxy colours, the bimodality of galaxy populations seems to be a fundamental property.

Many authors have attempted to quantify this “main sequence of star forming galaxies” through linear or model fitting (Noeske et al. 2007; Peng et al. 2010, Gilbank et al., submitted). Because our principal goal in this paper is to examine the differential evolution of group and field galaxies, we will avoid these kinds of parametric fits. However, visual inspection of this figure does yield at least two interesting features. First, the ‘main sequence’ in Figure 5 appears to have a steep slope, such that low mass galaxies have significantly higher SSFRs than do more massive galaxies. If we assume that this star forming sequence of galax-

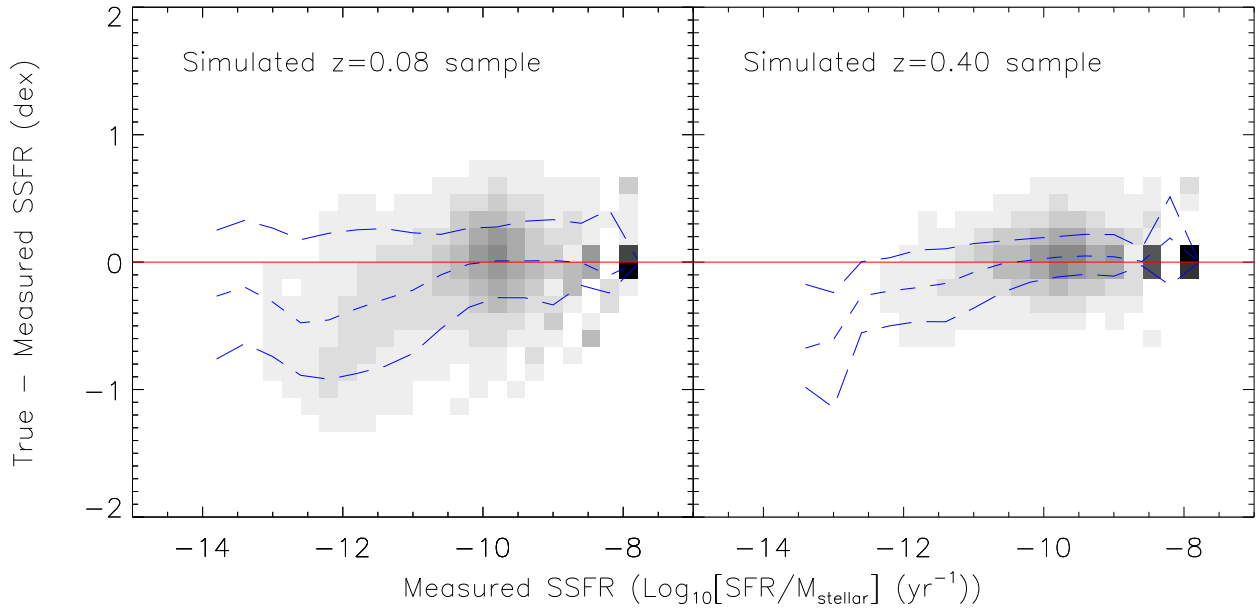


**Figure 4.** The difference between the "true" specific star formation rate of our mock galaxies and the results of the SED fitting as a function of the SED fit results. Again, this is shown for both samples, the  $z=0.08$  (left panel) and the  $z=0.4$  (right panel) simulated sample. The blue, central dotted line represents the running median of the offset, while the two blue, dashed lines show the  $1\sigma$  limits.

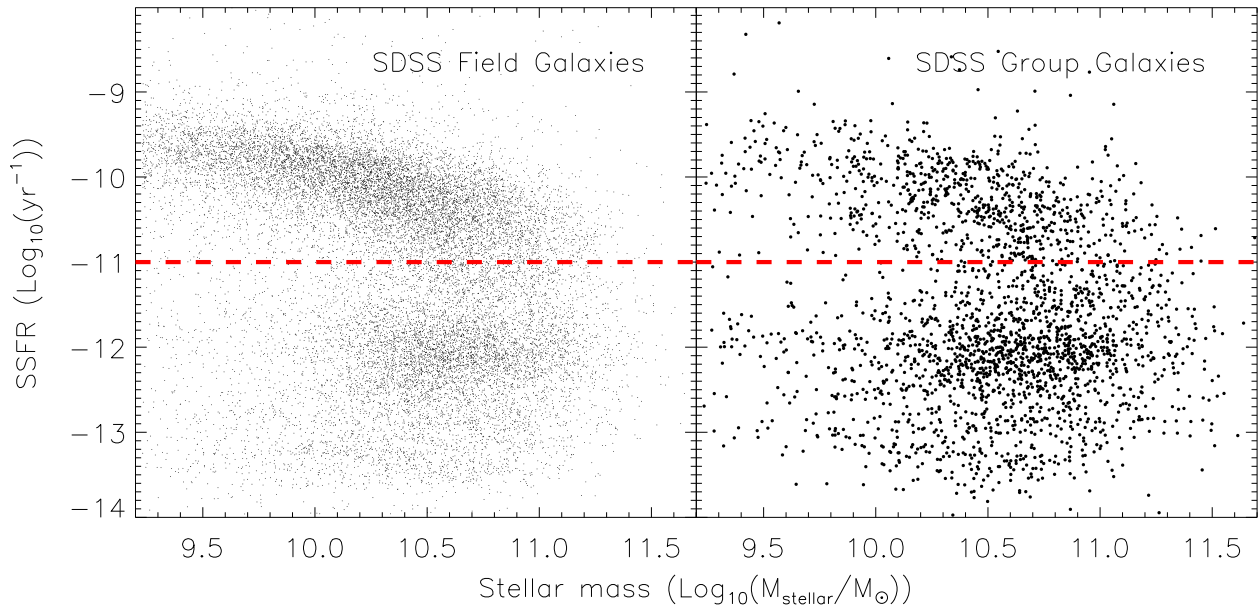


**Figure 5.** Specific star formation rates of both the group (right) and field (left) galaxies in the SDSS survey (median redshift 0.08) as a function of stellar mass. The dashed, red line corresponds to  $\log_{10} \text{SSFR} = 10^{-11} \text{yr}^{-1}$ , which is our division between active and passive galaxies. The typical uncertainty on SSFR is 0.31 dex, while the stellar mass uncertainty is 0.28 dex.

ies has always been star forming, then the massive galaxies have either formed earlier than less massive galaxies or have more rapidly declining star formation histories relative to less massive galaxies. Secondly, the slope and position of the group galaxies does not appear wildly different from the field galaxies. We will revisit this issue later.

We now move to higher redshift to examine the GEEC sample at  $z \sim 0.4$ . In Figure 6, we show the SSFR- $M_{\text{stellar}}$  plot for GEEC galaxies, separated into group and field environments. We only plot the stellar mass region in which we can create a statistically complete sample by applying the spatial, magnitude and  $1/V_{\text{max}}$  weights. As in the previous

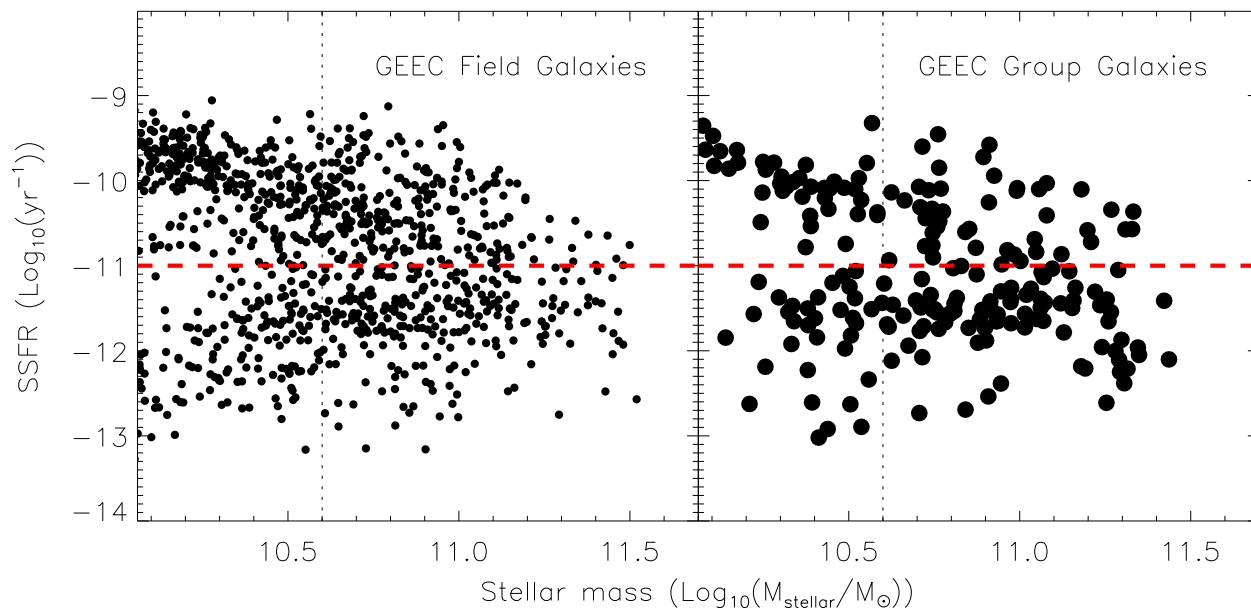


**Figure 6.** Specific star formation rates as a function of stellar mass for both the group (right) and field (left) galaxies in the GEEC survey (redshift = 0.4). The dashed, red line corresponds to  $\log_{10}\text{SSFR} = 10^{-11}\text{yr}^{-1}$ , which is our division between active and passive galaxies. The vertical, black, dotted line corresponds to the stellar mass limit ( $M_{\text{stellar}} = 3.9 \times 10^{10}$ ) at the highest redshift of the sample ( $z=0.55$ ). Using  $1/V_{\text{max}}$  weighting, we can obtain a complete sample to  $M_{\text{stellar}} = 1.44 \times 10^{10}$ , but the scatter plot does not reflect these weightings. The typical uncertainty on SSFR is 0.28 dex, while the stellar mass uncertainty is 0.19 dex.

figure, we see that it appears that galaxies form a sequence of star forming galaxies. Again, the sequence appears to have a tilt, such that massive galaxies have lower SSFRs than lower mass galaxies.

As was the case for the SDSS galaxies, it does not appear, via visual inspection of Figure 6, that the specific star formation rates of star forming galaxies are very different in groups compared with the field, in the GEEC sample. To quantify this and to evaluate the evolution with redshift, we present Figure 7 which shows the average SSFR of galaxies classified as star forming in both surveys. To avoid parametric forms, we simply assume that star forming galaxies are those with  $\log_{10}\text{SSFR} > 10^{-11}\text{yr}^{-1}$ . As shown by the red, dotted line in Figures 5 and 6, this appears to divide the star forming and passive galaxies at both redshifts. Further, a galaxy with this SSFR is forming stars at a fraction of its past average. This division is also useful because it implies that a galaxy forming stars at this SSFR with a mass of our GEEC stellar mass limit ( $\sim 10^{10} h^{-1} M_{\odot}$ ) would form stars at a rate of  $0.1 h^{-1} M_{\odot}/\text{yr}$ . Thus, the depth of UV photometry easily discriminates between star forming and passive galaxies.

Focusing first on the general field trends, shown by the black lines and symbols, we see that both the field samples in the GEEC survey and in the SDSS survey show steep trends with stellar mass. This behaviour was pointed out in the scatter plots earlier, but this confirms that the behavior remains when accounting for volume weighting of the surveys. We stress that this behavior is also not a result of a cut in star formation rate, as we are complete to the stellar mass limits shown. We notice that there is a significant offset in the SSFR- $M_{\odot}$  relation between surveys for

these star forming galaxies, such that star forming galaxies at redshift  $z=0.4$  were forming stars at higher rates ( $\sim 0.25$  dex in SSFR) than those at  $z=0.08$ . This offset is mass-independent for the mass ranges that are probed by both surveys ( $> 10^{10} M_{\odot}$ ).

Now, focusing on the group and field values within a given redshift, we see that, within the statistical uncertainties, there is no apparent difference. Thus, at least for the star forming galaxies, from  $z=0.4$  to  $z=0.08$ , we see a general lowering of the level of star formation in galaxies with no apparent mass dependence regardless of their environment.

#### 4.2 Fraction of passive galaxies

We have concentrated principally on the sequence of star forming galaxies and its position on the SSFR- $M_{\odot}$  plot. We now shift to look at what fraction of galaxies are within this sequence. As above, we define passive galaxies as those that have  $\log_{10}\text{SSFR} < 10^{-11}\text{yr}^{-1}$ . Figure 8 shows the passive fractions as a function of stellar mass for the group and field galaxies in both the SDSS survey and the GEEC survey. At both redshifts, we see that at all stellar masses probed, groups have a higher fraction of passive galaxies than the field. Given that this is comparing group galaxies with field galaxies at fixed stellar mass and redshift, it is strong evidence that group galaxies have star formation prematurely truncated by the group environment.

To guide the eye in Figure 8, we show a simple least square fit to each of the group and field passive fraction in SDSS. These two lines have very different slopes, implying that there is a mass dependent difference in the truncation mechanisms in the groups and the field. This is most inter-

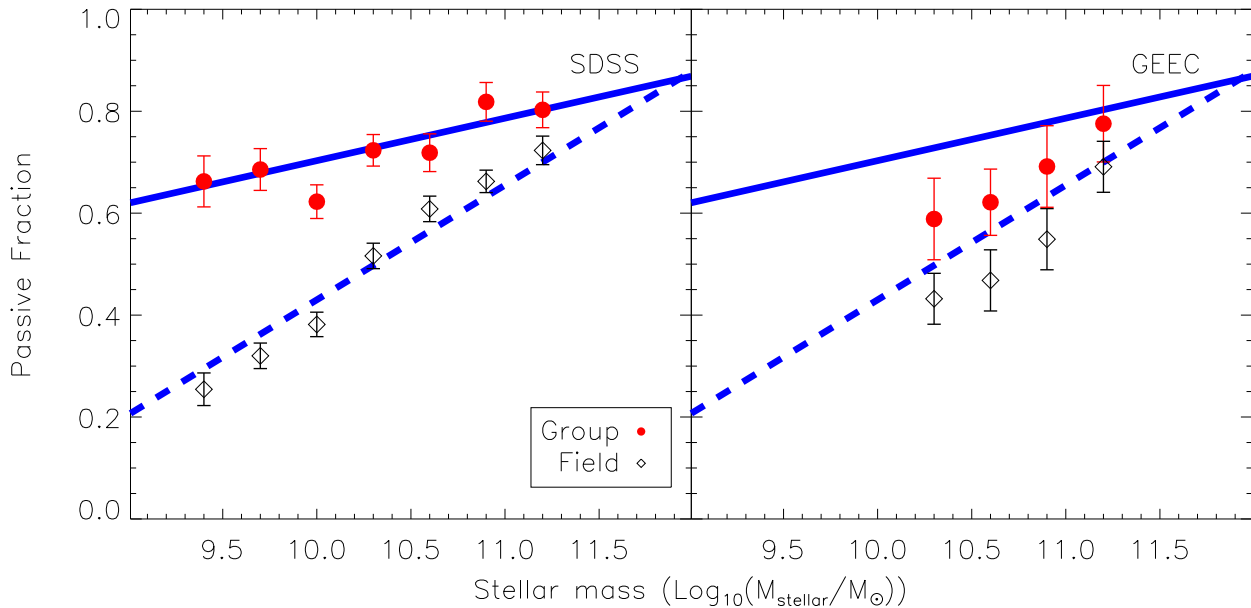


**Figure 8.** The fraction of passive galaxies in the group and field of SDSS (left panel) and GEEC (right panel) surveys. Passive galaxies have SSFRs less than  $10^{-11} \text{ yr}^{-1}$ . The solid blue line is an approximation to the mass dependence of the SDSS group galaxies, while the dashed blue line is an approximation to the SDSS field galaxies. For illustrative purposes, the same lines have also been reproduced in the GEEC panel. The error bars represent the error in the mean.

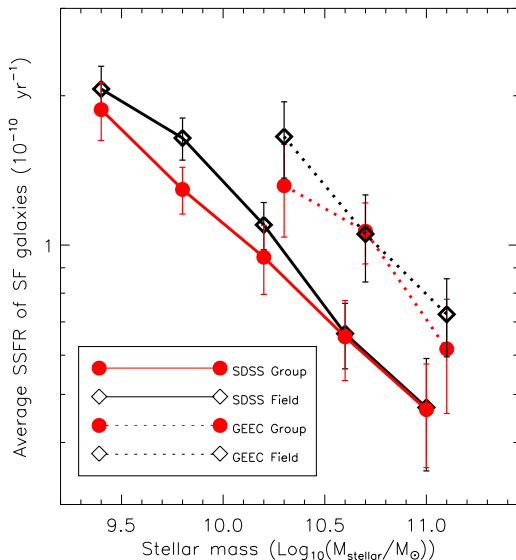


**Figure 7.** Average SSFR of star forming galaxies in the group and field of SDSS and GEEC surveys. Star forming galaxies are defined as being above  $\log_{10} \text{SSFR} > 10^{-11} \text{ yr}^{-1}$ , the red dashed line in Figures 5 and 6. The error bars represent the error in the mean.

esting when comparing to the GEEC sample. The SDSS lines have been re-drawn on the GEEC panel as well. This shows that the group and field galaxies at  $z=0.4$  have a mass dependent fraction with a similar slope to the SDSS field galaxies. Thus, the evolution in groups must be mass-dependent to

end with the correct fraction of passive galaxies in groups at  $z=0$ . This may be expected because in groups, the low mass galaxies are more likely to be satellites rather than central galaxies, and therefore, might experience the loss of their gas reservoir. These results are intriguing given our results in Figure 7, which showed that the average SSFR of star forming galaxies was similar in group and field at a given redshift. Galaxies must move quickly from being classed by our definition as ‘star-forming’ to ‘passive’ to cause the growing fraction of passive galaxies observed, while keeping the average SSFR of star forming galaxies unchanged.

## 5 DISCUSSION

### 5.1 Accretion model

In McGee et al. (2009), we introduced a simple approach for relating environmental effects to a galaxies accretion history. In this model, galaxies become ‘environmentally affected’ some time,  $T_{\text{trunc}}$ , after they fall into a host halo with a mass greater than  $M_{\text{trunc}}$ . It is important to note that our use of ‘environmentally affected’ does not necessarily mean, for example, red galaxies, because galaxies can also become red through internal processes. We are attempting to reproduce the *differential* effect of the group environment with time rather than making predictions for the group or field alone. Our model is based on the semi-analytic work of Font et al. (2008), but uses only the accretion history and stellar mass outputs. Our approach does not depend on the detailed star formation histories predicted by the Font et al. (2008) method. In Figure 9, we show the results for a model where  $T_{\text{trunc}} = 3 \text{ Gyrs}$  and  $M_{\text{trunc}} = 10^{13} M_{\odot}$ .

This shows the predictions for the environmentally affected fraction at  $z=0.08$  and  $z=0.4$ , as well as the observed group passive fractions at these redshifts. To match the overall SFR-determined passive fraction this model has a higher mass threshold than was shown previously by McGee et al. (2009), which had been determined to match optical 'red' fractions. However, as shown in McGee et al. (2009), the rate of evolution in these models is principally determined by  $T_{\text{trunc}}$ . While this model is simple, it is interesting to note that it predicts approximately the correct evolution in the passive fraction. Notice that at  $M_{\text{stellar}} = 10^{10.3} M_{\odot}$ , the evolution between the two redshift epochs in passive fractions is observed to be  $\sim 0.15$ . The model with a  $T_{\text{trunc}}$  of 3 Gyr agrees with this observed evolution. In contrast, a model with the same  $M_{\text{trunc}}$  but with  $T_{\text{trunc}} = 1$  Gyr predicts only an increase of 0.03. A timescale this short is disfavoured by the data, assuming that all galaxies in groups truncate with this timescale. As we have argued in McGee et al. (2009), the most powerful argument against a higher  $M_{\text{trunc}}$  is simply the observed difference in group and field passive fractions. A mechanism that occurs in the halo mass and timescale regime of our successful model could be strangulation, the relatively gentle process of removing the outer hot halo of infalling galaxies.

This accretion model is simplified in many ways and should only serve as a guide that the overall level of evolution seen in the data implies a long timescale. The galaxy formation model does not include the production of intragroup mass, which can be a significant fraction of the total stellar mass (McGee & Balogh 2010). Further, Kim et al. (2009) have shown that the inclusion of satellite-satellite merging and satellite-disruption to create intragroup mass improves the model's agreement with the luminosity dependent correlation function. The inclusion of these processes would likely create mass-dependent evolution since these process preferentially occur in low mass galaxies.

## 5.2 The role of environmental processes

We have seen that the sequence of star forming galaxies evolves with redshift, but that it is independent of environment. However, given that the fraction of star forming galaxies has such a strong environment dependence, we can ask the question: Are our results consistent with all low mass passive galaxies residing in massive halos? It is important to remember that our field sample is essentially the 'total' sample rather than an 'isolated' sample. The models of Font et al. (2008) show that 42% of galaxies are in halos above  $10^{12.75} M_{\odot}$  at  $z=0$  while at  $z=0.4$ , there are 26% of galaxies in these halos. Assuming that all of the galaxy groups have properties given by our sample, and the total population has the value of our 'field' data, we can infer the properties of 'isolated' galaxies, those in halos below  $10^{12.75} M_{\odot}$ . We can relate the group and field passive fractions ( $f_{\text{passive,group}}$ ,  $f_{\text{passive,field}}$ ) to the isolated passive fraction ( $f_{\text{passive,isolated}}$ ) using the fraction of galaxies in groups and those which are isolated fraction at that redshift ( $F_G$ ,  $F_I$ ), as

$$f_{\text{passive,isolated}} = \frac{f_{\text{passive,field}} - F_G * f_{\text{passive,group}}}{F_I}. \quad (3)$$

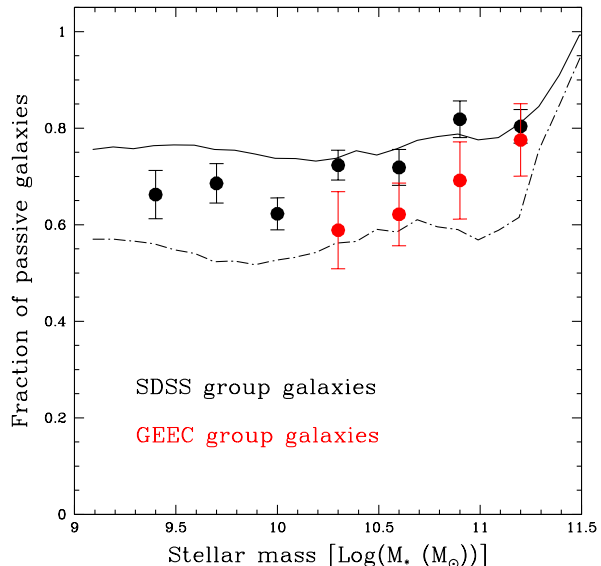


**Figure 9.** Comparison between the passive fraction of GEEC and SDSS group galaxies and a simple accretion model for environmental effects. Passive galaxies were determined via their specific star formation rates. The accretion model assumes that a galaxy become passive 3 Gyrs after it falls into a halo of at least  $10^{13} M_{\odot}$ . The solid black line is the prediction at the median redshift of SDSS,  $z=0.08$ , while the dashed black line is the model at  $z=0.4$ .

In this way, we see that the implied isolated passive fraction at  $M_{\text{stellar}} = 10^{11} M_{\odot}$  is 0.50 ( $\frac{0.55-0.26*0.69}{0.74}$ ) at  $z=0.4$  and is 0.56 ( $\frac{0.66-0.42*0.80}{0.58}$ ) at  $z=0$ . Thus, there is an intrinsic high passive fraction at this mass in isolated galaxies, but most of the evolution in the field between  $z=0.4$  and  $z=0$  is driven by the evolving group passive fraction. At  $M_{\text{stellar}} = 10^{9.4} M_{\odot}$ , for which we only have data at  $z=0$ , the implied true isolated fraction is essentially zero ( $\frac{0.27-0.42*0.66}{0.58}$ ). At lower mass, the field passive fraction appears to be entirely due to galaxy groups.

From this emerges a general picture in which massive galaxies have a high fraction of passive galaxies regardless of their environment, while low mass galaxies are essentially only passive in groups. This implies that massive galaxies must have an internal mechanism, or at least one that does not depend on environment, which plays a large role in the galaxy properties. On the other hand, low mass galaxies are essentially all star forming unless they are in a group or cluster environment. There have been models in which this internal mechanism is proposed to be the resultant heating caused by the fueling of active galactic nuclei (Springel et al. 2005; Hopkins et al. 2008).

It is perhaps surprising that we find most, if not all, of the low mass, passive galaxies can be accounted for if we assume they are only created in groups. This argument is based on CDM predictions of halo abundances and, while reasonably robust, does not rule out the possibility that some isolated galaxies in the real Universe may be passively evolving. Indeed, there is some evidence for such galaxies (eg., Malin & Carter 1983; Colbert et al. 2001; Zhu et al. 2010) although these tend to be more massive than our lowest mass galaxies. However, there is observational support in

the literature for this claim. In Baldry et al. (2006), only 5% of galaxies at the lowest stellar mass ( $10^9 M_\odot$ ) and in the lowest density region are on the red sequence. These authors also showed that, while on average the lowest density region hosts more isolated galaxies, there are a significant number of galaxies which are in group scale halos but which nonetheless appear to be in low density environments via their density indicator. Further, Haines et al. (2007), using the fourth data release of the Sloan Digital Sky Survey, find that none of the  $\sim 600$  galaxies in their lowest luminosity bin ( $-18 < M_r < -16$ ) and lowest density quartile are passive. Unfortunately, the literature can be misleading, because it is often convenient to call the lowest density bin of an observational sample 'isolated'. While this label is fine for the bulk properties, there can often be interlopers from groups or clusters, as Baldry et al. (2006) have shown. It has also been shown that a significant population of galaxies which appear isolated may be members of a 'backsplash' population, which have been through a massive halo and emerged on the other side (Gill et al. 2005). However, even after accounting for interlopers and backsplash galaxies, in apparent contradiction with Haines et al. (2007), Wang et al. (2009) have claimed that 30% of low luminosity ( $M_r > -17$ ) SDSS are red and isolated. The absence of a tight red sequence in these galaxies makes the division between red and blue galaxies difficult and is determined by an extrapolation of the luminosity dependent division of luminous galaxies. Given the lack of a tight red sequence, it is unclear whether a red  $g - r$  color as defined by these cuts is necessarily a passive galaxy and not a dust-reddened one. We note that the results of Haines et al., who determine passivity from the absence of  $H\alpha$  emission, are less sensitive to these problems.

It is worth noting that galaxy formation models, such as the semi-analytic models of Bower et al. (2006) and Croton et al. (2006), also predict that low mass passive galaxies are exclusively satellites of more massive galaxies in groups and clusters. In these models, the cessation of star formation in a galaxy occurs primarily through AGN feedback or satellite related processes.

One important question which arises is whether our results can be explained if galaxy evolution in groups is simply given a 'headstart'. That is, the galaxies within groups follow the same evolutionary path as isolated galaxies, but because of their dense environments they simply formed earlier and are thus further evolved. Simulations of dark matter haloes do show that there is a relationship at fixed halo mass between the age of the halo, or its epoch of formation, and its environment, such that haloes in a more biased environment form earlier (Gao et al. 2005; Wechsler et al. 2006; Maulbetsch et al. 2007; Li et al. 2008). Unfortunately, determining whether this bias dependent formation time of haloes at fixed *halo mass* leads to an environment-dependent formation time of galaxies at fixed *stellar mass* requires a more detailed understanding of galaxy formation. However, as we have seen in Figure 7, the average star formation rate at a given redshift is similar in the group and the field, but is significantly different at different redshifts. If galaxies simply ran out of gas, group galaxies would have different average star formation rates from field galaxies at the same redshift if they had a 'headstart'.

Further, it appears that most 'local' effects like AGN

correlate strongly with stellar mass (von der Linden et al. 2010). But controlling for stellar mass, we still see a higher passive fraction in groups. Although more work still needs to be done, this is strong evidence that galaxies have their star formation truncated in groups by an environment specific process.

## 6 CONCLUSION

We have fit spectral energy distributions to galaxies in two surveys, SDSS and GEEC. These SEDs use high quality, space based ultraviolet imaging along with optical, and near infrared for GEEC, photometry. We have compared this photometry to large suites of stellar population synthesis models to determine star formation rates and stellar masses. This method nicely reproduced alternative methods of measuring both star formation rates and stellar masses. By examining the results, we conclude the following.

- Star forming galaxies of all environments undergo a systematic lowering of their star formation rate between  $z=0.4$  and  $z=0.08$  regardless of mass.
- The star formation properties of star forming galaxies, as measured by their average specific star formation rates, are the same in the group and field environment at fixed redshift.
- The fraction of passive galaxies is higher in groups than the field at both redshifts. However, the difference between the group and field grows with time and is mass dependent, in the sense the the difference is larger at low masses.
- Low mass galaxies at  $z=0$  have group and field passive fractions that can be explained if passive galaxies only exist in groups.
- The evolution of passive fractions in groups between  $z=0.4$  and  $z=0$  is consistent with an accretion model in which galaxies are environmentally affected 3 Gyrs after falling into a  $10^{13} M_\odot$  halo/group.

These results present a consistent picture of environmental effects when taken along with our measurements of quantitative morphology in McGee et al. (2008). In that paper, we showed that the fraction of disk galaxies is higher in the field at both redshift and the difference grows larger with time. Also, we found that there was no indication that the disk scaling relations were different in the field or groups.

These results all suggest that only a fraction of galaxies in groups must be actively truncated at any given time. If the mechanism is a quick one, like ram pressure stripping, then the truncation time might be short enough that only a small fraction of group galaxies are affected at a given time. This would allow the bulk of the star forming galaxies to remain unchanged but still allow the observed evolution. However, ram pressure stripping is likely not effective in galaxy groups.

Based on the timescale suggested by our accretion model, strangulation seems like a suitable candidate for environmental mechanisms. However, it is unclear if strangulation can allow galaxies to remain apparently unaffected for some time, thereby appearing to act only on a fraction of group galaxies at a time. In semi-analytic models, strangulation produces too many 'green' galaxies, which would likely

alter the disk and star formation properties (Font et al. 2008; Balogh et al. 2009).

These results suggest that further constraints can be applied in two ways. First, the detailed study of individual galaxy groups and the orbits of their constituent galaxies within them can determine if ram pressure stripping of the cold gas is a viable mechanism. Secondly, the continued hunt for elusive ‘green’ transition galaxies, perhaps at high redshift where the accretion rates of galaxies into groups is higher (McGee et al. 2009; Balogh et al. 2010), will determine the viability of gentle, strangulation like mechanisms.

## ACKNOWLEDGMENTS

We thank the referee for a thorough and constructive report. MLB and LCP acknowledge support from NSERC Discovery Grants. We would also like to thank the original CNOC2 redshift survey team, who allowed us access to their unpublished redshifts. This paper is based on observations made with the NASA Galaxy Evolution Explorer under GO program 37 and archival data from the 3rd General Release. GALEX is operated for NASA by California Institute of Technology under NASA contract NAS-98034. This work is based in part on data products produced at the TERAPIX data center located at the Institut d’Astrophysique de Paris. Some of the data presented in this paper were obtained from the Multimission Archive at the Space Telescope Science Institute (MAST). Support for MAST for non-HST data is provided by the NASA Office of Space Science via grant NAG5-7584 and by other grants and contract. Observations used in this paper were obtained with WIRCam, a joint project of CFHT, Taiwan, Korea, Canada, France, at the Canada-France-Hawaii Telescope (CFHT) which is operated by the National Research Council (NRC) of Canada, the Institut National des Sciences de l’Univers of the Centre National de la Recherche Scientifique of France, and the University of Hawaii. Funding for the creation and distribution of the SDSS Archive has been provided by the Alfred P. Sloan Foundation, the Participating Institutions, the National Aeronautics and Space Administration, the National Science Foundation, the US Department of Energy, the Japanese Monbukagakusho, and the Max Planck Society.

## REFERENCES

- Adelman-McCarthy, J. K. et al. 2008, *ApJS*, 175, 297  
 Allard, F. & Hauschildt, P. H. 1995, *ApJ*, 445, 433  
 Alongi, M., Bertelli, G., Bressan, A., Chiosi, C., Fagotto, F., Greggio, L., & Nasi, E. 1993, *A&ASS*, 97, 851  
 Baldry, I. K., Balogh, M. L., Bower, R. G., Glazebrook, K., Nichol, R. C., Bamford, S. P., & Budavari, T. 2006, *MNRAS*, 373, 469  
 Baldry, I. K., Glazebrook, K., Brinkmann, J., Ivezić, Ž., Lupton, R. H., Nichol, R. C., & Szalay, A. S. 2004, *ApJ*, 600, 681  
 Baldwin, J. A., Phillips, M. M., & Terlevich, R. 1981, *PASP*, 93, 5  
 Balogh, M. L., Baldry, I. K., Nichol, R., Miller, C., Bower, R., & Glazebrook, K. 2004, *ApJL*, 615, L101  
 Balogh, M. L. & McGee, S. L. 2010, *MNRAS*, 402, L59  
 Balogh, M. L. et al. 2007, *MNRAS*, 374, 1169  
 —. 2009, *MNRAS*, 398, 754  
 —. 2010, arXiv:1011.5509  
 Bell, E. F. 2002, *ApJ*, 577, 150  
 Bertin, E. & Arnouts, S. 1996, *A&AS*, 117, 393  
 Bertin, E., Mellier, Y., Radovich, M., Missonnier, G., Dideon, P., & Morin, B. 2002, in *Astronomical Society of the Pacific Conference Series*, Vol. 281, *Astronomical Data Analysis Software and Systems XI*, ed. D. A. Bohlender, D. Durand, & T. H. Handley, 228–+  
 Bessell, M. S., Brett, J. M., Scholz, M., & Wood, P. R. 1991, *A&ASS*, 89, 335  
 Bessell, M. S., Brett, J. M., Wood, P. R., & Scholz, M. 1989, *A&ASS*, 77, 1  
 Blanton, M. R., Lin, H., Lupton, R. H., Maley, F. M., Young, N., Zehavi, I., & Loveday, J. 2003, *AJ*, 125, 2276  
 Blanton, M. R. & Moustakas, J. 2009, *ARA&A*, 47, 159  
 Boselli, A. & Gavazzi, G. 2006, *PASP*, 118, 517  
 Bower, R. G. et al. 2006, *MNRAS*, 370, 645  
 Bressan, A., Fagotto, F., Bertelli, G., & Chiosi, C. 1993, *A&ASS*, 100, 647  
 Brinchmann, J. et al. 2004, *MNRAS*, 351, 1151  
 Bruzual, G. & Charlot, S. 2003, *MNRAS*, 344, 1000  
 Budavári, T. et al. 2009, *ApJ*, 694, 1281  
 Calzetti, D., Armus, L., Bohlin, R. C., Kinney, A. L., Koornneef, J., & Storchi-Bergmann, T. 2000, *ApJ*, 533, 682  
 Carlberg, R. G. et al. 2001, *ApJ*, 552, 427  
 Chabrier, G. 2003, *PASP*, 115, 763  
 Charlot, S. & Fall, S. M. 2000, *ApJ*, 539, 718  
 Chary, R. & Elbaz, D. 2001, *ApJ*, 556, 562  
 Colbert, J. W., Mulchaey, J. S., & Zabludoff, A. I. 2001, *AJ*, 121, 808  
 Cortese, L., Boselli, A., Franzetti, P., Decarli, R., Gavazzi, G., Boissier, S., & Buat, V. 2008, *MNRAS*, 386, 1157  
 Croton, D. J. et al. 2006, *MNRAS*, 365, 11  
 Dale, D. A. & Helou, G. 2002, *ApJ*, 576, 159  
 Fagotto, F., Bressan, A., Bertelli, G., & Chiosi, C. 1994a, *A&ASS*, 104, 365  
 —. 1994b, *A&ASS*, 105, 29  
 Finoguenov, A. et al. 2009, *ApJ*, 704, 564  
 Font, A. S. et al. 2008, *MNRAS*, 389, 1619  
 Fukugita, M., Shimasaku, K., & Ichikawa, T. 1995, *PASP*, 107, 945  
 Gao, L., Springel, V., & White, S. D. M. 2005, *MNRAS*, 363, L66  
 Gilbank, D. G., Baldry, I. K., Balogh, M. L., Glazebrook, K., & Bower, R. G. 2010a, *MNRAS*, 405, 2594  
 Gilbank, D. G., Balogh, M. L., Glazebrook, K., Bower, R. G., Baldry, I. K., Davies, G. T., Hau, G. K. T., Li, I. H., & McCarthy, P. 2010b, *MNRAS*, 405, 2419  
 Gill, S. P. D., Knebe, A., & Gibson, B. K. 2005, *MNRAS*, 356, 1327  
 Haines, C. P., Gargiulo, A., La Barbera, F., Mercurio, A., Merluzzi, P., & Busarello, G. 2007, *MNRAS*, 381, 7  
 Hopkins, A. M. 2004, *ApJ*, 615, 209  
 Hopkins, P. F., Cox, T. J., Kereš, D., & Hernquist, L. 2008, *ApJS*, 175, 390  
 Huchra, J. P. & Geller, M. J. 1982, *ApJ*, 257, 423  
 Ivezić, Ž. et al. 2004, *Astronomische Nachrichten*, 325, 583  
 Kauffmann, G. et al. 2003, *MNRAS*, 341, 33



- . 2004, MNRAS, 353, 713
- Kennicutt, Jr., R. C. 1983, ApJ, 272, 54
- Kennicutt, Jr., R. C., Tamblyn, P., & Congdon, C. E. 1994, ApJ, 435, 22
- Kim, H., Baugh, C. M., Cole, S., Frenk, C. S., & Benson, A. J. 2009, MNRAS, 400, 1527
- Kimm, T. et al. 2009, MNRAS, 394, 1131
- Kroupa, P. 2001, MNRAS, 322, 231
- Le Borgne, J. et al. 2003, A&A, 402, 433
- Lemaux, B. C., Lubin, L. M., Shapley, A., Kocevski, D., Gal, R. R., & Squires, G. K. 2010, ApJ, 716, 970
- Li, Y., Mo, H. J., & Gao, L. 2008, MNRAS, 389, 1419
- Lilly, S. J., Le Fevre, O., Hammer, F., & Crampton, D. 1996, ApJL, 460, L1+
- Madau, P., Ferguson, H. C., Dickinson, M. E., Giavalisco, M., Steidel, C. C., & Fruchter, A. 1996, MNRAS, 283, 1388
- Malin, D. F. & Carter, D. 1983, ApJ, 274, 534
- Martin, D. C. et al. 2005, ApJL, 619, L1
- Maulbetsch, C., Avila-Reese, V., Colín, P., Gottlöber, S., Khalatyan, A., & Steinmetz, M. 2007, ApJ, 654, 53
- McCarthy, I. G. et al. 2008, MNRAS, 383, 593
- McGee, S. L. & Balogh, M. L. 2010, MNRAS, 403, L79
- McGee, S. L., Balogh, M. L., Bower, R. G., Font, A. S., & McCarthy, I. G. 2009, MNRAS, 400, 937
- McGee, S. L., Balogh, M. L., Henderson, R. D. E., Wilman, D. J., Bower, R. G., Mulchaey, J. S., & Oemler, A. J. 2008, MNRAS, 387, 1605
- Meurer, G. R., Heckman, T. M., Leitherer, C., Kinney, A., Robert, C., & Garnett, D. R. 1995, AJ, 110, 2665
- Morrissey, P. et al. 2007, ApJS, 173, 682
- Moustakas, J., Kennicutt, Jr., R. C., & Tremonti, C. A. 2006, ApJ, 642, 775
- Noeske, K. G. et al. 2007, ApJL, 660, L43
- Oke, J. B. & Gunn, J. E. 1983, ApJ, 266, 713
- Parker, L. C., Hudson, M. J., Carlberg, R. G., & Hoekstra, H. 2005, ApJ, 634, 806
- Peng, Y. et al. 2010, ApJ, 721, 193
- Puget, P. et al. 2004, Proc. SPIE, 5492, 978
- Rieke, G. H., Alonso-Herrero, A., Weiner, B. J., Pérez-González, P. G., Blaylock, M., Donley, J. L., & Marcillac, D. 2009, ApJ, 692, 556
- Salim, S. et al. 2007, ApJS, 173, 267
- . 2009, ApJ, 700, 161
- Scalo, J. M. 1986, Fundamentals of Cosmic Physics, 11, 1
- Schlegel, D. J., Finkbeiner, D. P., & Davis, M. 1998, ApJ, 500, 525
- Springel, V., Di Matteo, T., & Hernquist, L. 2005, MNRAS, 361, 776
- Stoughton, C. et al. 2002, AJ, 123, 485
- Strateva, I. et al. 2001, AJ, 122, 1861
- Strauss, M. A. et al. 2002, AJ, 124, 1810
- Tran, K. et al. 2009, ApJ, 705, 809
- von der Linden, A., Wild, V., Kauffmann, G., White, S. D. M., & Weinmann, S. 2010, MNRAS, 404, 1231
- Wang, Y. et al. 2009, ApJ, 697, 247
- Wechsler, R. H., Zentner, A. R., Bullock, J. S., Kravtsov, A. V., & Allgood, B. 2006, ApJ, 652, 71
- Weinmann, S. M., van den Bosch, F. C., Yang, X., & Mo, H. J. 2006, MNRAS, 366, 2
- Werner, M. W. et al. 2004, ApJS, 154, 1
- Wilman, D. J., Balogh, M. L., Bower, R. G., Mulchaey, J. S., Oemler, A., Carlberg, R. G., Morris, S. L., & Whitaker, R. J. 2005, MNRAS, 358, 71
- Wilman, D. J., Oemler, A., Mulchaey, J. S., McGee, S. L., Balogh, M. L., & Bower, R. G. 2009, ApJ, 692, 298
- Wilman, D. J., Zibetti, S., & Budavári, T. 2010, MNRAS, 406, 1701
- Wilman, D. J. et al. 2008, ApJ, 680, 1009
- Yan, R., Newman, J. A., Faber, S. M., Konidaris, N., Koo, D., & Davis, M. 2006, ApJ, 648, 281
- Yee, H. K. C. et al. 2000, ApJS, 129, 475
- York, D. G. et al. 2000, AJ, 120, 1579
- Zhu, G., Blanton, M. R., & Moustakas, J. 2010, ApJ, 722, 491

## APPENDIX A: UNDERSTANDING THE PHYSICAL PARAMETERS

In this appendix, we attempt to determine how well our SED fit galaxy parameters reproduce the values given by alternative methods. We will compare our SDSS stellar masses and star formation rates with the publicly available results of Kauffmann et al. (2003, K03; for stellar masses) and Brinchmann et al. (2004, B04; for star formation rates). We also compare our GEEC stellar masses to those determined primarily from  $K$  band data by Balogh et al. (2007).

### A1 SDSS comparisons: Stellar Masses

The method of fitting stellar masses used by K03, is the philosophical forerunner of the Bayesian method we use here, with much of the formalism explained in that paper. The authors use a large suite of galaxy models created using stellar population synthesis, and find that they can constrain the  $z$  band mass to light ratios using the 4000-Å break ( $D_n(4000)$ ) and the Balmer absorption line index  $H\delta_A$ . By then scaling by the observed  $z$  band photometry, they determine the galaxy's stellar mass. Thus, despite the similar methodology, the K03 stellar masses are largely determined by the spectral features, which determine the star formation history and thus the mass to light ratio. In contrast, our stellar masses are determined by using the UV light to constrain the star formation histories and then the optical/NIR photometry to scale to a stellar mass.

In Figure A1, we show the difference between our stellar masses and those of K03 as a function of our stellar mass. The K03 masses have been converted from a Kroupa (2001) to a Chabrier IMF by dividing by 1.04. The masses are well reproduced using our method, with a scatter that is smaller than the average of the uncertainties in either method. This likely means that despite our different methods, the uncertainties on each method are correlated. Nonetheless, our SED fitting seems to produce reliable results, notwithstanding systematic issues common in both methods (ie. evolving IMF, stellar population synthesis uncertainties, etc.).

### A2 SDSS comparisons: Star formation rates

One of the most common and robust methods of determining star formation rates of star forming galaxies is to use the recombination emission line  $H\alpha$ , which re-radiates the

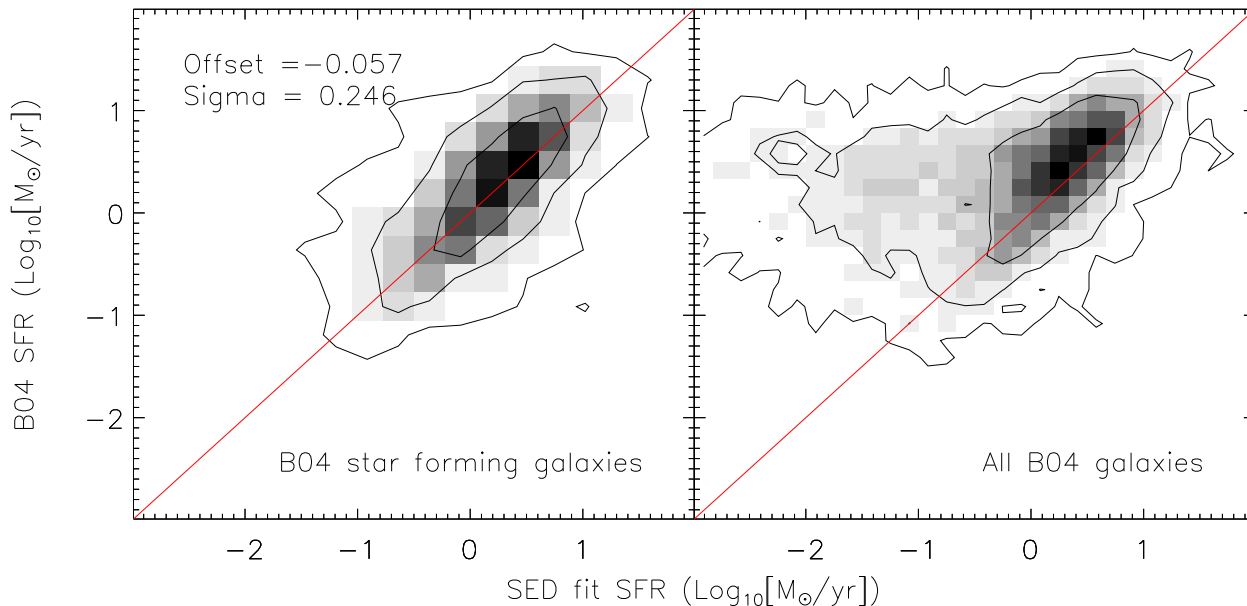


**Figure A2.** A comparison between the SED fit star formation rates in this paper and those found by Brinchmann et al. (2004, B04). We show this for galaxies that B04 classifies as “star-forming” in the left panel and all galaxies in the right panel. The red line shows the equality between the B04 and SED fit star formation rates.

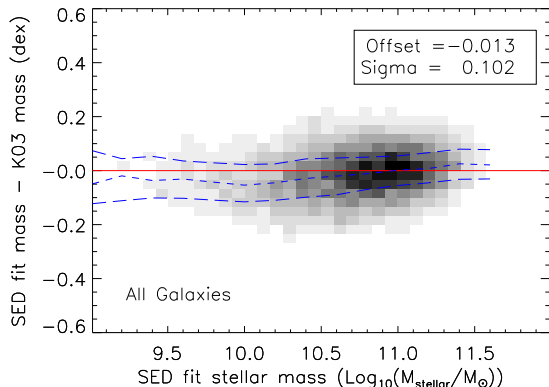


**Figure A1.** The difference between the SED fit masses presented in this paper and those based on Kauffmann et al. (2003, K03). The masses are well reproduced using our method. The red line represent the equality of the masses, while the blue dashed lines show the median and 1 sigma upper and lower bounds of the distribution.

radiation of massive young stars. To that end, B04 use the emission lines of SDSS galaxies, to both classify the type of galaxy and to determine the star formation rates. As this method is completely based on spectral features this should give essentially an independent measurement to ours.

B04 classifies galaxies into several categories based on the position of the galaxy within the Baldwin et al. (1981, BPT) diagram and the quality of the spectra. The BPT diagram is used to determine whether a galaxy has AGN activity based on the ratios of four emission lines ([OIII]5007, H $\beta$ , [NII]6584 and H $\alpha$ ). A galaxy with a high signal-to-noise

ratio in each emission line and that lies in the star forming locus of the BPT diagram is defined as a “star forming” galaxy. The other B04 categories are used to denote AGN or Composite galaxies, as well as low S/N categories of each.

The star formation rate of high signal-to-noise star forming galaxies is relatively straightforward to obtain from emission lines. Thus, it is this class of galaxies that we first compare our SED fit star formation rates to, as shown in the left panel of Figure A2. The B04 star formation rates were calculated assuming a Kroupa (2001) initial mass function. Following Salim et al. (2007), we have divided the B04 rates by 1.06 to account for this difference in IMF. Our measurement agrees very well, with only a negligible offset and a 1  $\sigma$  value that is consistent with our expected measurement errors. Importantly, some of this scatter is likely real, given that the B04 SFRs are based on H $\alpha$ , which is sensitive to star formation within the last 10 Myrs, while our SFRs are based on *NUV*, which is sensitive star formation in the last 100 Myrs. An additional source of possible scatter arises because the SDSS survey spectra, which are made by a fiber based spectrograph, only sample the central 1/3 of the total galaxy light at the median redshift. Although B04 attempts to correct these aperture effects by using the available photometry, these will likely add further scatter when compared to our method of using total magnitudes alone.

The right panel of Figure A2 shows the comparison of our SFRs with all of the galaxies for which B04 determined SFRs and are in the *GALEX* sample. In other words, in addition to those galaxies B04 classified as star forming, this panel also includes galaxies classified as AGN, composite or low S/N. While the SED fit high star formation rates still agree well with the B04 measurements, there is a long tail of SED fit determined low star formation rates that in B04 are forming stars at much higher rates. Salim et al. (2007) also

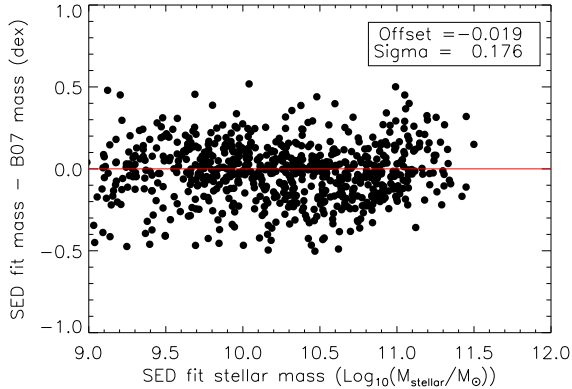


**Figure A3.** Comparison between the SED fit stellar masses in this paper and the  $K$ -band determined Balogh et al. (2007)(B07) masses for galaxies in both catalogs in the redshift range  $0.1 < z < 0.55$ . The  $1\sigma$  scatter is 0.176 dex, and the SED fit stellar masses are systematically lower by 0.019 dex (ie.  $\sim 2\%$ ).

noted this behavior when comparing UV derived SFR with B04. Salim et al. extensively investigate this phenomenon and find that these galaxies are ones in which B04 used indirect SF indicators, either because of lack of  $H\alpha$  emission or because of AGN contamination of the nebular emission lines. Thus, as Salim et al. conclude, the UV SED fit SFR are likely more accurate for these galaxies. Further, the indirect methods used by B04 (ie.  $D_n(4000)$ -based) measure SFRs over different timescales than the Balmer lines, and our UV-based method.

### A3 GEEC comparisons: Stellar Masses

In Balogh et al. (2007), we determined stellar masses for a limited sample of GEEC galaxies based on the  $K$  band data that was available at the time. These were determined by computing  $K$  band mass to light ratios using simple stellar population modeling. The authors use a young, constantly star forming galaxy model to approximate the most blue galaxies ( $B - V < 0.4$ ) and a old, single stellar population model for the reddest galaxies ( $B - V > 1$ ). The mass to light ratios for intermediate galaxies are determined by a linear interpolation between these two extremes based on the galaxy's  $B-V$  color.

In Figure A3, we present a comparison between our current SED fit stellar masses and those of B07. We have converted from a Salpeter IMF to a Chabrier IMF by subtracting 0.21 dex. Encouragingly, there is only a slight offset of -0.019 between the masses and the scatter is quite small  $0.176\sigma$ . This scatter is actually smaller than the formal errors of both mass measurements, but since they are, at least partially, using the same photometry, the errors are correlated.